Energy 275 (2023) 127437

Contents lists available at ScienceDirect

Energy

journal homepage: www.elsevier.com/locate/energy

Irreversible losses, characteristic sizes and efficiencies of sCO_2 axial turbines dependent on power capacities

Tianze Wang [a], Jinliang Xu [a,b,*], Zhaofu Wang [a], Haonan Zheng [a], Jianhui Qi [c], Guanglin Liu [a,b]

[a] Beijing Key Laboratory of Multiphase Flow and Heat Transfer for Low Grade Energy Utilization, North China Electric Power University, Beijing, 100026, China
[b] Key Laboratory of Power Station Energy Transfer Conversion and System (North China Electric Power University), Ministry of Education, Beijing, 102206, China
[c] Shandong Engineering Laboratory for High-efficiency Energy Conservation and Energy Storage Technology & Equipment, Shandong University, Jinan, Shandong, 250061, China

ARTICLE INFO

Keywords:
sCO_2 cycle
Turbine efficiency
Irreversible loss
Scaling law

ABSTRACT

Supercritical carbon dioxide (sCO_2) cycle can be driven by fossil energy and solar/nuclear energy. Available references maximize cycle efficiency by fixing turbine efficiencies η_{tt} in advance. Here, we provide turbine efficiencies dependent on power capacities W_T which are in the range of (50–450) MW. After examination of working mechanism and special characteristic of sCO_2 turbines, a comprehensive model was presented to predict characteristic sizes, irreversible losses and efficiencies of turbines. Characteristic size of turbines (l_c) is found to obey the scale law of $l_c \sim W_T^{0.5}$. Profile loss Y_p, secondary loss Y_s, clearance loss Y_{cl} and trailing edge loss Y_{te} obey the scaling laws of $Y_p \sim W_T^{-0.075}$, $Y_s \sim W_T^{-0.075}$, $Y_{cl} \sim W_T^{-0.39}$, $Y_{te} \sim W_T^{-1}$. These scaling laws agree with the correlations based on numerical simulations. With continuous increase of W_T, η_{tt} increases but the slope of the curves become gentle. Efficiency maps are provided based on inlet pressures P_{in} and temperatures T_{in}. By fixing W_T, η_{tt} decreases with increase of P_{in} and T_{in}. The scaling laws regarding irreversible losses provide the guidance to optimize the turbine design. The efficiency maps can be integrated in the cycle analysis for accurate estimate of system performance, and help to select suitable power capacity.

1. Introduction

Supercritical carbon dioxide Brayton cycle, called sCO_2 cycle, was initially proposed by Sulzer in 1950 [1]. Since then, it was not paid much attention. In the last decade, great efforts have been put to develop sCO_2 cycle, which is expected to be applied in power plants driven by fusel energy (coal and nature gas), solar energy, nuclear energy, flue gas waste heat [2–4]. The sCO_2 cycle has higher efficiency than water-steam based Rankine cycle, reducing CO_2 emission when generating a specific amount of electricity. Besides, sCO_2 cycle has simple cycle configuration and compact components, yielding fast response adapting to external load variations. In China, there will be a long time for the electric grid to be operating in a mixing mode including fossil energy, renewable energy and nuclear energy [5]. The water-steam Rankine cycle slowly responds to load variations, but sCO_2 cycle significantly increases the load variation speed, balancing various energy sources to create robust and smart grid [5].

sCO_2 turbines are key components that convert thermal energy into power. Because thermal properties of sCO_2 are different from water and organic fluids, design, construction and operation of sCO_2 turbines have distinct characteristics [6]. Xu et al. commented on the progress made on sCO_2 turbines [5]. USA (Sandia National Lab, Southwest Research Institute, Echogen, GE, Net Power), Japan (TIT), Korea (KIER) and China (North China Electric Power University, Xian Thermal Power Research Institute, Institute of Engineering Thermophysics) have built several sCO_2 loops [7–9]. Bearing, sealing and rotor-dynamics stability have been paid great attention. It is shown that the ideal gas assumption introduces errors to estimate various losses in sCO_2 turbines. The real gas effect should be considered for better design and operation of sCO_2 turbines [10]. KIER built test loop with two types of turbo-generator with a conventional carbon mechanical seal and oil-lubricated tilting bearings [8]. SwRI and GE are developing a new film-riding face seal design, restricting CO_2 leakage from supercritical pressure to near-atmospheric pressure with shaft speeds up to 3600 r/min [11]. SwRI and GE are developing ~10 MWe scale turbomachines [6]. A clean-sheet conceptual design of a 450 MWe assembled turbine rotor is presented [11]. China is developing a 5 MW sCO_2 test loop driven by

* Corresponding author. Beijing Key Laboratory of Multiphase Flow and Heat Transfer for Low Grade Energy Utilization, North China Electric Power University, Beijing, 100026, China.
E-mail address: xjl@ncepu.edu.cn (J. Xu).

https://doi.org/10.1016/j.energy.2023.127437
Received 9 July 2022; Received in revised form 15 January 2023; Accepted 2 April 2023
Available online 6 April 2023

Nomenclature

A	entrance area (m^2)
a	axial chord length (m)
b	blade height (m)
c	chord length (m)
C	cost ($)
C_L	lift coefficient
d_m	average radius (m)
D	hub radius (m)
F	flaring angle (°)
F_{AR}	aspect ratio correction factor
h	enthalpy (J/kg)
k_{mod}	design technology correction factor
k_{inc}	off-design correction factor
k_p	Mach number factor considering Y_p
k_s	Mach number factor considering Y_s
k_{Re}	Reynolds number correction factor
L	axial turbine length (m)
l_c	characteristic length of turbine (m)
m	mass flow rate (kg/s)
Ma	Mach number
n	rotating speed (r/min)
N	number of stage
w	blade throat (m)
P	pressure (MPa)
p	blade pitch (m)
Q	volume flow rate (m^3/s)
R	degree of reaction
Re	Reynolds number
r	radius (m)
s	entropy (kJ/kg)
T	temperature (°C)
t	trailing edge thickness (m)
t_{max}	maximum blade thickness (m)
U	peripheral velocity (m/s)
V	absolute velocity (m/s)
V_x	meridional velocity (m/s)
W	relative velocity (m/s)
W_{net}	power capacity of cycle (MW)
W_T	power capacity of turbine (MW)
Y_S	loss in stator
Y_R	loss in rotor
Y_p	profile loss
Y_{p1}	profile loss in nozzle blades
Y_{p2}	profile loss in impulse blades
Y_s	secondary loss
$\widetilde{Y}_s$	preliminary estimate of secondary loss
Y_{cl}	clearance loss
Y_{te}	trailing edge loss
Y_{ex}	supersonic expansion loss
Y_{sh}	shock loss
Z	Ainley loading parameter
z	the number of blades
N_s	specific speed
D_s	specific diameter

Greek symbols

ΔP_{total}	total turbine pressure drop (MPa)
ΔP_S	pressure drop in stator (MPa)
ΔP_R	pressure drop in rotor (MPa)
ΔP_{loss}	pressure drop due to losses (MPa)
α	absolute flow angle (°)
α_m	mean flow angle (°)
β	relative flow angle (°)
γ	stagger angle (°)
ξ	α_1/α_2
μ	viscosity (Pa·s)
λ	hub to tip radius ratio
φ	flow coefficient
ψ	loading coefficient
η_{tt}	isentropic efficiency (%)
σ	solidity
ρ	density (kg/m^3)
$\overline{\varepsilon}$	residual error
ε	expansion pressure ratio
δ	radial clearance (m)
ϕ	diameter (m)

Subscripts

1, 2, 3 … 7	node
S	stator
R	rotor
in	turbine inlet
out	turbine outlet

Abbreviations

C1, C2, C3	compressor
DRH	double-reheating
IC	intercooling
RC	recompression cycle
SC	simple Brayton cycle
TC	tri-compression cycle
T1	high-pressure turbine
T2	moderate-pressure turbine
T3	low-pressure turbine

nature gas, which has been put into operation [12]. It is shown that demonstration of sCO_2 cycles is success, in which small scale (10 kWe−1 MWe) radial flow turbomachines are applied. Thermal efficiencies are usually smaller than the designed value due to various issues such as leakage [8].

Radial turbines for sCO_2 cycle have been widely investigated in recent years, including one-dimension efficiency estimation [13], numerical simulations [14,15], experiment demonstration and performance test [16,17]. These turbines are suitable for small scale power capacities such as below 10 MWe [18]. We note that sCO_2 cycles can be driven by various heat sources, under which large scale power generation is required. For these applications, power plants with power capacities in the range of (10∼1000) MWe are welcome. For example, coal fired power plants have the power capacities in the range of (300–1000) MWe, in which ∼300 MWe capacity belongs to small scale applications [19]. For solar energy applications, the suitable power capacity may be (50–100) MWe [20].

In the past five years, China has performed the concept design and component demonstration of 1000 MWe sCO_2 coal fired power plant [21–23]. The purpose of the project is to reach higher efficiency using sCO_2 cycle instead of the widely used water-steam based Rankine cycle, reducing the carbon dioxide emission. Challenges exist on the coupling of the sCO_2 boiler and the cycle. To eliminate the pressure drop penalty, modular boiler was proposed to suppress the pressure drops induced by ultra-large flow rate due to using sCO_2 as the working fluid [21]. To extract flue gas energies over entire temperature range, the hybrid cycles including a top sCO_2 cycle and a bottom sCO_2 cycle were proposed [24]. The components sharing technique integrates the two cycles into a

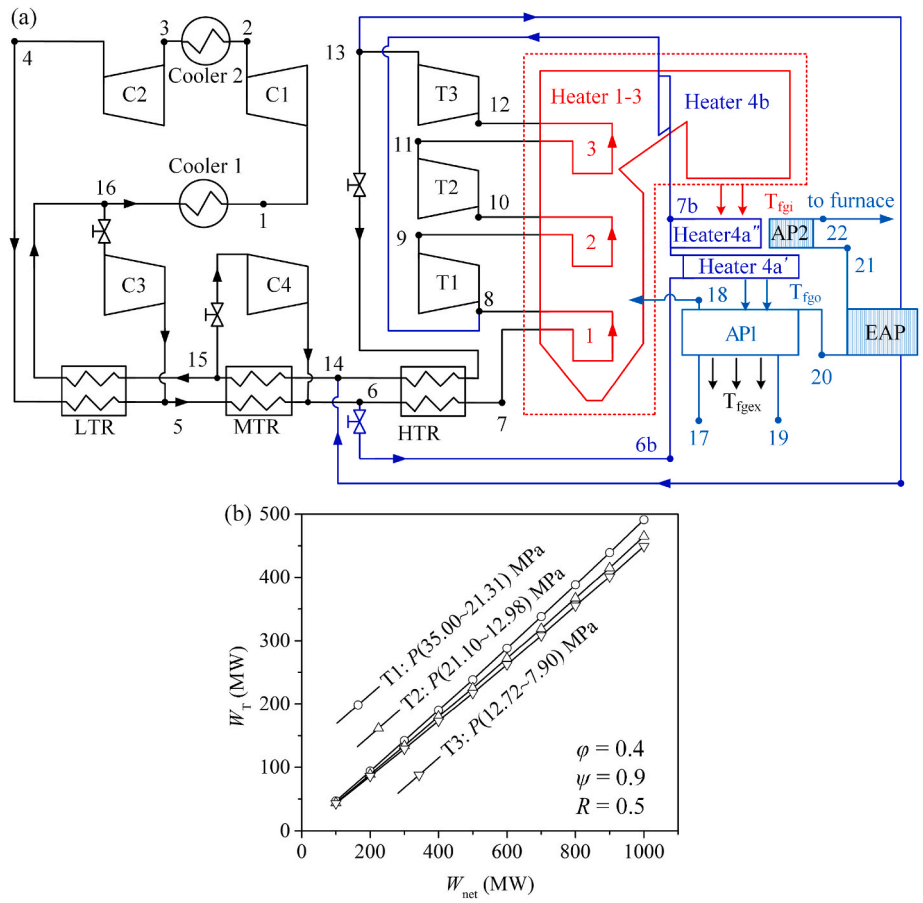

Fig. 1. Connection of sCO_2 cycle and turbines. (a) The 1000 MWe sCO_2 coal fired power plant design, embedding the tri-compression cycle, double-reheating, intercooling and overlap energy utilization. This figure is replotted based on Ref. [34]. (b) Powers of three turbines versus power capacity of power plant.

single one, simplifying the system layout [25]. A series of works have been done on the three axial turbines adapting to the 1000 MWe net power output, including the parameters and configuration design, numerical simulations, and a package solution of issues such as sealing, cooling and others [26–28]. The project reached the target of the net power efficiency of 51.03%, which is higher than the advanced water-steam based Rankine cycle power plant of ~47%. This target saves 140,000 tons of standard coal and reduces the CO_2 emission by 290,000 tons in a fiscal year. To verify the proposed theoretical/numerical works for the power plant, Numerical simulation and calculation have been performed for sCO_2 boiler, turbine, and printed circuit heat exchangers [22,26,29].

The above works were performed for a rated power capacity of 1000 MWe. The present paper provides a one-dimensional efficiency estimation of sCO_2 turbines, adapting to the power capacity of the power plant in a wide range of (100–1000) MWe. Such a study helps select a suitable power capacity (below 1000 MWe) that will have comprehensive performance of higher efficiency and acceptable cost. Thus, the flexible operation of coal fired power plant increases, increasing the utilization ratio of solar energy and wind energy. Three axial turbines are included in the cycle, dividing into three groups of high-pressure, moderate-pressure and low-pressure, consecutively. Considering other cycle types and heat source such as solar energy, effects of design parameters of inlet pressure, temperature and expansion ration are also explored. Results are presented for turbine efficiencies dependent on power capacities. Efficiency maps are also provided in terms of inlet pressures and temperatures.

We note that most of the literature pays attention to cycle configuration and design parameters that maximizes the cycle efficiency, but neglects the turbine design features that are necessary to obtain them, by fixing the turbine efficiency in advance [22,30]. This may overestimate the system efficiency [5]. The turbine efficiency results obtained in this paper can be integrated in the cycle analysis, increasing the reliability of the analysis. Turbine (expander) efficiencies are well documented by Lio et al. [31,32] for organic Rankine cycle. Turbine efficiencies dependent on power capacities for sCO_2 cycle are not found. Various irreversible losses exist in axial turbines to influence turbine efficiencies. The losses models of expanders with organic fluids should be reexamined for sCO_2 turbines.

The present paper is organized as follows. Section 2 establishes a connection between the cycle and the turbines. Section 3 describes the model to determine turbine efficiencies dependent on power capacities, including 4 subsections. Section 3.1 refers to the theoretical background, section 3.2 refers to the calculation procedure for turbine efficiency, section 3.3 describes the loss model for axial flow turbines, section 3.4 refers to the validation of the model. Section 4 reports the results and discussion. Conclusions are summarized in section 5.

2. The connection of power capacities between power plant and turbines

This section tries to provide a connection between power capacities of power plant and those of turbines. Thus, one can understand the power capacity for each turbine that should be undertaken to contribute a power capacity of the power plant. We started from a short description of the 1000 MWe sCO_2 coal fired power plant (see Fig. 1a), then a linear assumption is made between power capacities of the cycle and the power capacity for each turbine. Because investigations have been reported for the 1000 MWe sCO_2 coal fired power plant [21,22,33], we summarize the key techniques that are necessary to reach the net power

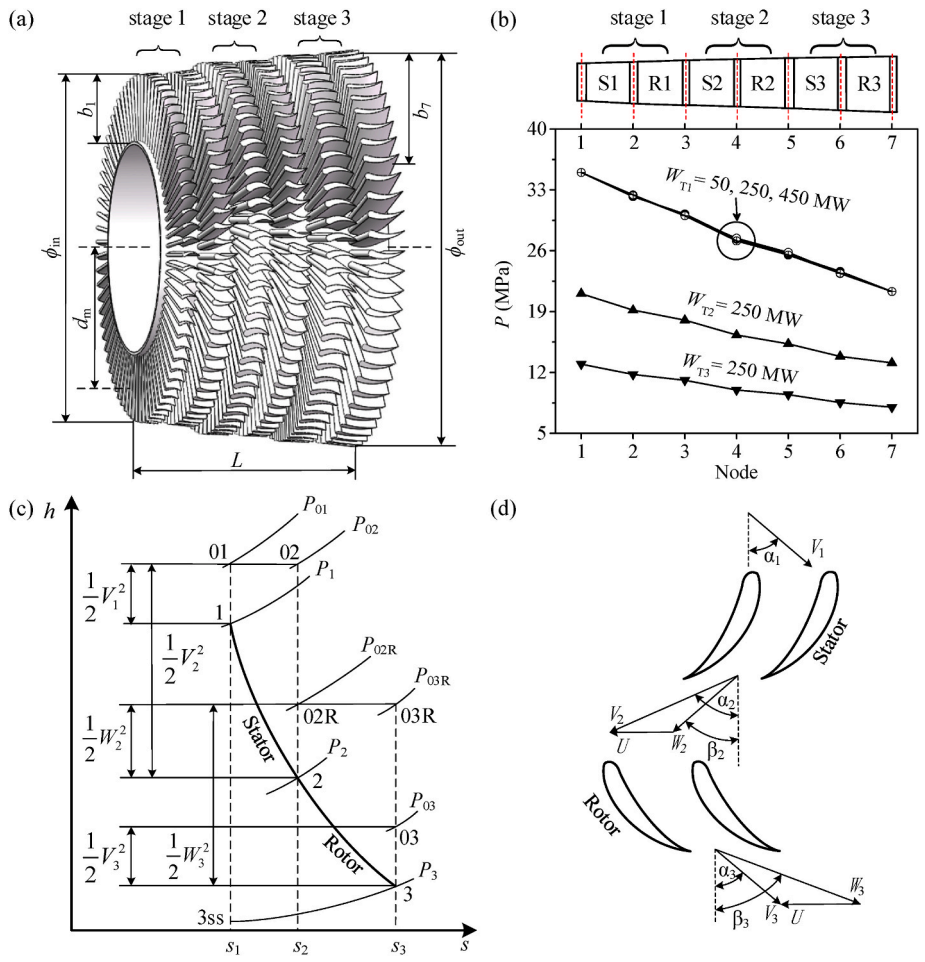

Fig. 2. Physical picture showing the expansion process in axial flow turbines. (a) The overall sizes for axial turbines. (b) Pressure decreases along the axial flow direction. (c) The *h-s* diagram in the first stage of turbine. (d) Velocity triangles due to expansion.

efficiency of 51.03%.

2.1. Tri-compression sCO2 cycle

Recompression cycle (RC) is widely used [34]. Ref. [35] commented on that the synergies of the two compression processes in RC ensures the improved cycle efficiency compared with a single compression cycle (SC). Based on synergetics, multi-compression sCO_2 cycle was further proposed. Tri-compression cycle (TC) is regarded as a RC cooperating with a SC. The synergies of RC and SC has better efficiency of TC than RC [35]. TC is recommended to be applied for coal fired power plant [35]. In Fig. 1a, C1 and C2 are two compressors but regarded as a single one. Splitting a single compressor into two and adding the cooler 1 represent the intercooling technique (IC) to reduce the compression work. The four compressors of C1, C2, C3 and C4 reflect the TC cycle used. Adding a compressor also requires an additional regenerator heat exchanger. Hence, three regenerators of HTR, MTR and LTR are included in Fig. 1a.

2.2. Double-reheating technique

For water-steam based Rankine cycle, reheating or double-reheating are helpful to improve the power plant efficiency [21]. Such techniques are also embedded in sCO_2 cycle (see Fig. 1a). The sCO_2 at the turbine T1 outlet is further heated in boiler and then enters turbine T2 for power generation. Such process is repeated for T3. Hence, double-reheating (DRH) is called.

2.3. Overlap energy utilization of flue gas energies

sCO_2 cycle is suitable for temperatures of heat source higher than 550 °C. Challenge exists on the extraction of flue gas energies over the entire temperature range (1500 °C–120 °C) for boiler applications. The hybrid cycle was proposed to contain a top sCO_2 cycle and a bottom sCO_2 cycle. The top cycle, bottom cycle and the air-preheater account for the whole energy absorption, satisfying the cascade energy utilization principle [36]. Because the bottom cycle has lower efficiency than the top cycle, an overlap region is set in high temperature region of flue gas. Flue gas energies in the overlap region is not only absorbed by the top cycle, but also by the bottom cycle. The average absorption temperature of the bottom cycle increases to increase its efficiency [36]. After utilization of the overlap energy utilization, various components (not all) share similar pressure and temperature parameters but they have different flow rates of sCO_2, the two cycles can be combined into a single one. In Fig. 1a, Heater 4a' and Heater 4a" are the heat exchangers to absorb flue gas heat in the overlap region for top cycle and bottom cycle, respectively.

A comprehensive thermal hydraulic model was established for the cycle computation shown in Fig. 1a. The isentropic efficiencies of three turbines are coupled with the cycle efficiency and they are iteratively determined. Procedures for the calculation of 1000 MWe power plant were documented in Refs. [22,36,37] and they are not repeated here. For the vapor parameters of 630 °C/35 MPa at the turbine T1 inlet, the net power efficiency reaches 51.03%, which is apparently higher than that of the advanced water-steam based Rankine cycle power plant. For the W_{net} = 1000 MWe net power generation, the powers for the three

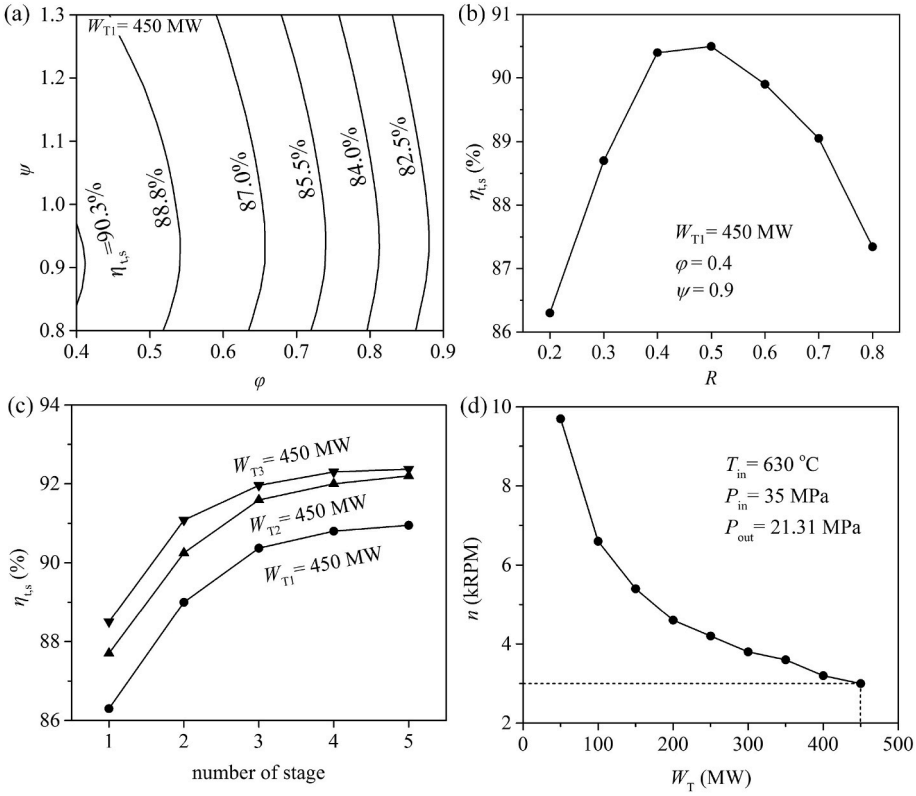

Fig. 3. Effect of various parameters on turbine performance.(Default design parameters: $\varphi = 0.4$, $\psi = 0.9$, $R = 0.5$, $N = 3$, $n = 3000$ r/min) (a) The isentropic efficiency of turbine T1 at 450 MW dependent on load coefficient and flow coefficient. (b) The isentropic efficiency of turbine T1 at $W_{T1} = 450$ MW, $\varphi = 0.4$, $\psi = 0.9$ dependent on degree of reaction. (c) Effect of number of stages on turbine efficiencies. (d) The rotating speed versus the power capacities of turbine T1.

turbines are W_{T1} = 491 MW, W_{T2} = 465 MW and W_{T3} = 449 MW, respectively. There are three coefficients connecting cycle power and turbine power: $W_{T1} = c_1 W_{net}$, $W_{T2} = c_2 W_{net}$ and $W_{T3} = c_3 W_{net}$. Based on the outcomes of W_{net} = 1000 MWe, c_1, c_2 and c_3 are 0.491, 0.465 and 0.449, respectively. Assuming constant cycle performance at different power capacities, the c_1, c_2 and c_3 make links between cycle power and turbine power (see Fig. 1b). The three turbines operate in same design parameters ($\varphi = 0.4$, $\psi = 0.9$, $R = 0.5$) and in different pressure levels, which are (35 MPa~21.31 MPa) for T1, (21.10 MPa~12.98 MPa) for T2, and (12.72 MPa~7.90 MPa) for T3. Thus, they are called high-pressure turbine, moderate-pressure turbine and low-pressure turbine, respectively. For the following presentations, we focus on efficiencies and irreversible losses for the three turbines dependent on their own power capacities, instead of the power capacity of the cycle.

3. Turbine efficiencies dependent on power capacities

Salah et al. [38] presented sCO_2 axial turbine computations with single-stage expansion, in which mass flow rate is set as a given parameter. Here, a comprehensive sCO_2 axial turbine mode is presented to determine the turbine efficiency. Extended from the Salah et al. model [38], our model deals with multi-stages turbine. Power capacity is set as a design parameter. Mass flow rate is determined by iterating turbine power and its efficiency, instead of a given parameter. Our work is also referenced to the works of Lio et al. [31,32] for organic Rankine cycles.

3.1. Theoretical background

Compared with turbines with steam-water or organic fluid as working fluid, the sCO_2 turbine has distinct characteristics. Because the turbine operates at pressures higher than the critical pressure, the sCO_2 expansion displays high fluid density feature, ensuring much smaller size compared with low density fluid expansion in water-steam turbines and organic fluid turbines. Taking three-stages turbine as an example, the overall sizes are characterized by two diameters of ϕ_{in} and ϕ_{out} at the inlet and outlet planes, respectively, two blade heights of b_1 and b_7 at the inlet and outlet planes, respectively, the whole axial length of L, and an average radius of d_m (see Fig. 2a). Each stage contains a stator and a rotor, in which enthalpy is constant in stator, and enthalpy drops to convert thermal energy into power in rotor. Various nodes such as 1–7 are marked along the axial length (see Fig. 2b). The computation needs to determine thermodynamic parameters at each node location. Pressures decrease along the axial length due to expansion.

Fig. 2c plots the enthalpy-entropy (h-s) diagram in the first stage of the turbine. The isentropic expansion from node 1 to node 3 is demonstrated by the dashed line from 1 to 3ss. An actual expansion is expressed by solid curve from 1 to 3 due to the entropy rise. The isentropic efficiency is

$$\eta_{t,1} = \frac{h_1 - h_3}{h_1 - h_{3ss}} \tag{1}$$

Where h is the enthalpy, the subscript 1 refers to the expansion in the first stage. The work generation is

$$W_{T,1} = m(h_1 - h_3) \tag{2}$$

Where m is the mass flow rate. Referring to Fig. 2c for h-s curve and Fig. 2d for velocity triangle, total pressures are defined at the three node locations, with the subscript marked as $0i$, where i is the node number. For example, at node 2, P_{02} is written as

$$P_{02} = f\left(h_2 + \frac{V_2^2}{2}, s_2\right) \tag{3}$$

Where the term $h_2 + \frac{V_2^2}{2}$ is called the total enthalpy, V_2 is the absolute

velocity. Another "total pressure" P_{02R} is defined by total enthalpy characterized by the relative velocity W_2, instead of V_2 (see Fig. 2d).

$$P_{02R} = f\left(h_2 + \frac{W_2^2}{2}, s_2\right) \tag{4}$$

Similar definitions can be written for node 1 and node 3. It is noted that P_{01} exists but P_{01R} does not exist due to no relative velocity at node 1. In Fig. 2d, α and β are the absolute flow angle and relative flow angle, respectively. The degree of reaction is defined as

$$R = \frac{h_2 - h_3}{h_1 - h_3} \tag{5}$$

Fig. 2c indicates that only after the thermodynamic parameters at node 1 and node 3 are determined, the expansion efficiency and work production can be determined, involving the iteration calculation of P_2.

For three-stages expansion, after all the thermodynamic parameters at various nodes are determined, the total-to-total efficiency for the whole turbine is written as

$$\eta_{tt} = \frac{h_1 - h_7}{h_1 - h_{7ss}} \tag{6}$$

The work generation by the whole turbine is

$$W_T = m(h_1 - h_7) \tag{7}$$

Referring to axial turbine with organic fluids [31,32,39] and considering the special expansion characteristics of sCO_2 turbine, the total-to-total turbine efficiency is expressed as

$$\eta_{tt} = f(\varphi, \psi, R, W_T, N, n, Ma, P_{in}, P_{out}, T_{in}, Y_S, Y_R) \tag{8}$$

$$\varphi = \frac{V_x}{U}, \psi = \frac{h_1 - h_3}{U^2} \tag{9}$$

Where φ, ψ and R are flow coefficient, loading coefficient and degree of reaction, respectively. W_T is the power output for the whole turbine, N is the number of stages, n is the rotating speed, Ma is the Mach number, P_{in} and T_{in} are pressure and temperature defined at the turbine inlet condition corresponding to node 1, P_{out} is the pressure at the turbine outlet condition, for three-stages turbine, it refers to the value at node 7, Y_S and Y_R are the losses in stator and rotor, respectively. The losses shall contain the summary information for all the stages of turbine, V_x is the meridional velocity and U is the peripheral velocity. Effects of these parameters are commented here.

The values of φ and ψ have important effect on turbine performance. Usually, the combination of a smaller φ and a larger ψ yields a higher turbine efficiency [40]. For 1000 MWe coal fired sCO_2 cycle, the efficiency of turbine T1 attains maximum with $\varphi = 0.4$ and $\psi = 0.9$ ($R = 0.5$), under which $W_{T1} = 450$ MW. Thus $\varphi = 0.4$ and $\psi = 0.9$ are used in this study (see Fig. 3a). The R reflects the enthalpy drop in rotor relative to that in the whole stage. Each stage has its corresponding R value. Equation (5) writes R during the first stage expansion. For three-stages expansion, R for the second stage and third stage expansion write

$$\begin{cases} R = \dfrac{h_4 - h_5}{h_3 - h_5} & \text{for second stage} \\ R = \dfrac{h_6 - h_7}{h_5 - h_7} & \text{for third stage} \end{cases} \tag{10}$$

Here, we use the same R for all the three stages expansion. Based on Ref. [32], when φ and ψ reach 0.4 and 0.9, respectively, R is suggested to be in the range of 0.45–0.50. Our calculation results shown in Fig. 3b are consistent with the suggestions by Ref. [32]. Hence, we set $R = 0.5$ in this paper.

Multi-stages expansion is used for large scale power generation, decreasing the load for each stage of the turbine. Fig. 3c shows the total-to-total efficiencies of the three turbines of high-pressure, moderate-pressure and low-pressure. The η_{tt} increases with increase of the number of stages (N), but the slope decreases beyond $N = 3$. The selection of N is balanced by turbine efficiency and fabrication cost. Ref. [41] gives the turbine cost as

$$C_T = \frac{479.34m \times \ln(\epsilon) \times (1 + e^{0.036T_{in} - 54.4})}{0.93 - \eta_{tt}} \tag{11}$$

Where ϵ is the expansion pressure ratio, defined as P_{in}/P_{out}. The calculation based in Eq. (11) indicates that the cost increases by 35% when using four stages expansion compared with using three stages expansion. Hence, we use the three stages expansion in this paper. Refs. [5,33] suggests that it is better to choose three stages expansion for 1000 MWe power generation of the coal fired power plant. The three stages expansion is also used for other power capacities except 1000 MWe of the power plant.

Attention is paid to the rotating speed of the turbine (n). Small scale (1–10 MWe) sCO_2 turbines operate at very high speed [42]. The turbine efficiency increases with increase of n [43]. The determination of n needs two parameters of N_S (specific speed) and D_S (specific diameter) [44].

$$N_S = \frac{n\sqrt{Q}}{(h_1 - h_{7ss})^{3/4}} = \text{constant} \times \frac{\varphi^{1/2}}{\psi^{3/4}} \tag{12}$$

$$D_S = \frac{2d_m(h_1 - h_{7ss})^{1/4}}{\sqrt{Q}} = \text{constant} \times \frac{\psi^{1/4}}{\varphi^{1/2}} \tag{13}$$

Where h_{7ss} is the enthalpy at the turbine outlet (node 7 outlet), based on isentropic expansion, Q is the volume flow rate, d_m is the average diameter (see Fig. 2a). Once φ and ψ are known, the determination of n needs two constants in Eqs.(12) and (13). The n strongly depends on power capacities of turbines. In China, the alternating current of electricity is 50 Hz frequency. If the n is regulated to 3000 r/min by turbine itself, it is not necessary to use gearbox. If n is larger than 3000 r/min, gearbox is needed to adapt the rotating speed to 3000 r/min, satisfying the electricity frequency of 50 Hz [11]. For the $W_{net} = 1000$ MWe net power generation, the powers for the three turbines are $W_{T1} = 491$ MW, $W_{T2} = 465$ MW and $W_{T3} = 449$ MW. Based on Ref. [11], it is not convenient to use gearbox for a single turbine larger than 450 MW. Thus $n = 3000$ r/min is directly used for all the three turbines of the 1000 MW power plant. Substituting $n = 3000$ r/min and corresponding Q at 450 MW into Eqs.(12) and (13) yields the two constants. Using the determined constants, the n can be calculated at other power capacities. Fig. 3d plots the n versus W_T, showing the sharp rise of n when W_T decreases. The n at $W_T = 50$ MW is about three times of that at $W_T = 450$ MW.

Mach number influences thermal-power conversion for low density fluid expansion such as encountered in water-steam turbines [45]. The sCO_2 turbines operate at pressures higher than the critical value, the Ma number is small thus its effect can be neglected.

The P_{in} and T_{in} are the maximum pressure and temperature entering the first turbine of the cycle, which depend on the heat source. For coal fired power plant, P_{in} is high such as (30–35) MPa [22]. T_{in} depends on the tolerance temperature of materials, which is ~630 °C for water-steam Rankine cycle, and is being increased to ~700 °C level [5]. These considerations are also suitable for sCO_2 cycle. For solar/nuclear energy utilizations, P_{in} can be ~20 MPa or ~16 MPa [46], which is lower than that for coal fired power plant. The turbine efficiency map will be presented on P_{in}-T_{in} plane in the Results and Discussion section. The P_{out} depends on the number of turbines in the cycle. When using reheating or double-reheating, two or three turbines are used. For the last turbine, P_{out} can be slightly higher than the critical pressure of CO_2. Effects of Y_S and Y_R will be commented in Section 3.3.

Because multi-stages expansion is used, assumptions are made as follows: (1) The φ, ψ and R are identical for different stages, (2) The enthalpy drop is the same for different stages:

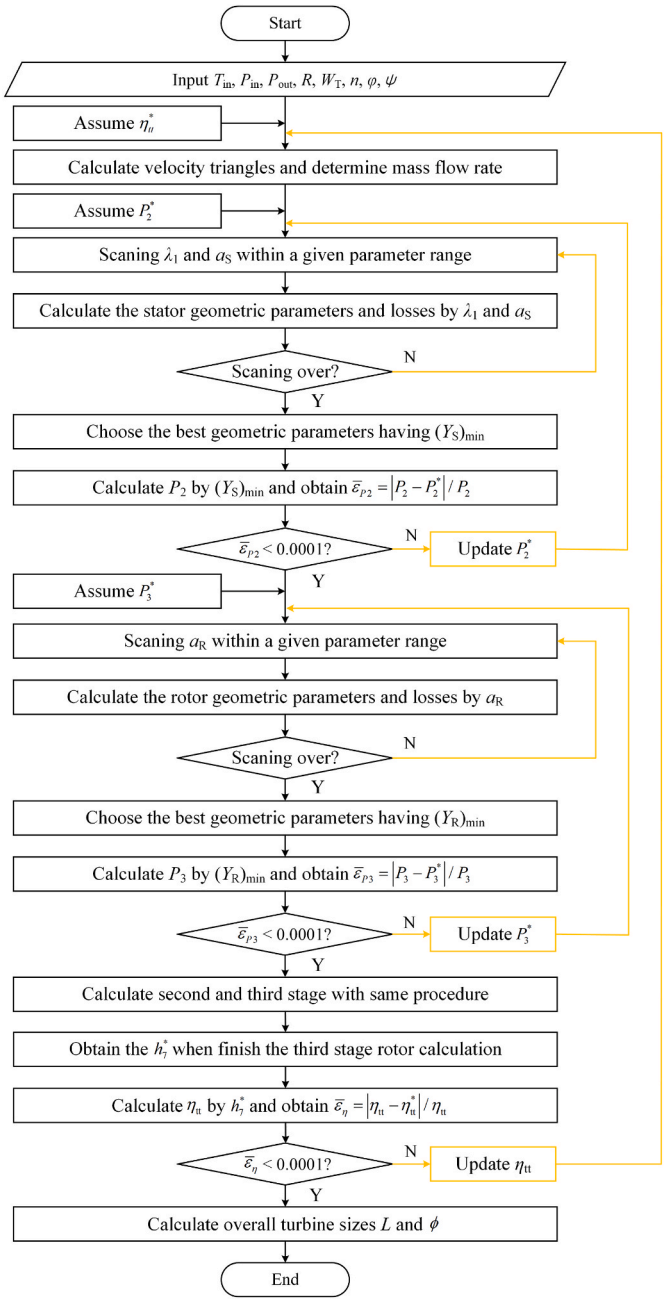

Fig. 4. Calculation procedure for axial flow turbines.

$$h_1 - h_3 = h_3 - h_5 = h_5 - h_7 \tag{14}$$

(3) The peripheral velocity U and meridional velocity V_x are the same for different stages, (4) Flow angles of α and β are the same for different stages. However, due to the expansion with decreased densities along axial direction, geometrical sizes increase stage by stage. The efficiencies are different for different stages.

3.2. The calculation procedure for turbine efficiency

Fig. 4 shows the calculation procedure for turbine efficiency. The three levels of iteration refer to turbine efficiency, pressures at each node location, and geometry parameters, respectively. Initially, a turbine efficiency η_{tt}^* is assumed. Combining P_{out} (it is P_7 for three-stages expansion) and Eq. (6), one knows the state parameters at the outlet condition. The mass flow rate m is determined by Eq. (7). Enthalpies at each node are calculated as

$$h_3 = h_1 - \frac{(h_1 - h_7)}{3}, h_5 = h_3 - \frac{(h_1 - h_7)}{3} \tag{15}$$

$$\begin{cases} h_2 = h_3 + R(h_1 - h_3) \\ h_4 = h_5 + R(h_3 - h_5) \\ h_6 = h_7 + R(h_5 - h_7) \end{cases} \tag{16}$$

Then, U and V_x are determined as

$$U = \sqrt{(h_1 - h_3)/\psi}, V_x = U\varphi \tag{17}$$

Referring to Fig. 2d, the velocity triangles are calculated as [44].

$$\begin{cases} \alpha_2 = \arctan\left(\dfrac{1 - R + \psi/2}{\varphi}\right), \alpha_3 = \arctan\left(\dfrac{1 - R - \psi/2}{\varphi}\right) \\ \beta_2 = \arctan\left(\dfrac{-R - \psi/2}{\varphi}\right), \beta_3 = \arctan\left(\dfrac{-R + \psi/2}{\varphi}\right) \end{cases} \tag{18}$$

$$\begin{cases} V_2 = V_x/\cos\alpha_2, V_3 = V_x/\cos\alpha_3, V_1 = V_3 \\ W_2 = V_x/\cos\beta_2, W_3 = V_x/\cos\beta_3 \end{cases} \tag{19}$$

Further calculations obey the following procedures.

Stator calculation: Combining an assumed P_2^* at node 2 and h_2 achieves all the thermodynamics parameters at node 2. The area at the entrance location A_1 is

$$A_1 = \frac{m}{\rho_1 V} \tag{20}$$

The determination of various geometry parameters for stator needs to search the optimal condition. A set of combinations of axial chord length a_S and hub to tip radius ratio λ_1 are assumed. The geometry parameters are [31].

$$d_m = \sqrt{\frac{2}{\pi}\frac{1 + \lambda_1^2}{1 - \lambda_1^2}A_1} \tag{21}$$

$$D_S = \sqrt{\frac{2}{1 + \lambda_1^2}}\lambda_1 d_m, b_S = \frac{D_S}{\lambda_1 - D_S} \tag{22}$$

$$c_S = a_S \cos\gamma, p_S = \frac{c_S}{\sigma}, w_S = p_S \cos\beta_2, z_S = \frac{2\pi d_m}{p_S} \tag{23}$$

$$t_S = \max(0.05 w_S, 1), \delta_S = 0 \tag{24}$$

Where D is the hub radius, b is the blade height, c is the chord length, p is the pitch distance between neighboring blades, w is the blade throat, z is the number of blades, t is the trailing edge thickness, the subscript S means stator. Fig. 5a–b shows the definitions of various geometry parameters.

By searching the minimum losses for stator, one determines the final a_S and λ_1 as well as the corresponding geometry sizes. The P_{02} and loss in stator (Y_S) are

$$P_{02} = f\left(h_2 + \frac{V_2^2}{2}, s_2\right), Y_S = \frac{P_{01} - P_{02}}{P_{02} - P_2} \tag{25}$$

The calculation of stator is thought to be converged if

$$\bar{\varepsilon}_{P2} = \left|\frac{P_2 - P_2^*}{P_2}\right| \le 0.0001 \tag{26}$$

Table 2 lists reasonable ranges of various parameters, which are modified from the recommendation values based on Ref. [47]. If the determined values are beyond the scope of the corresponding ranges, the group parameters that come from the combination set of a_S and λ_1 are eliminated.

Rotor calculation: Similar procedure is performed for rotor. An initial P_3^* is assumed to decide the thermodynamics parameters at node

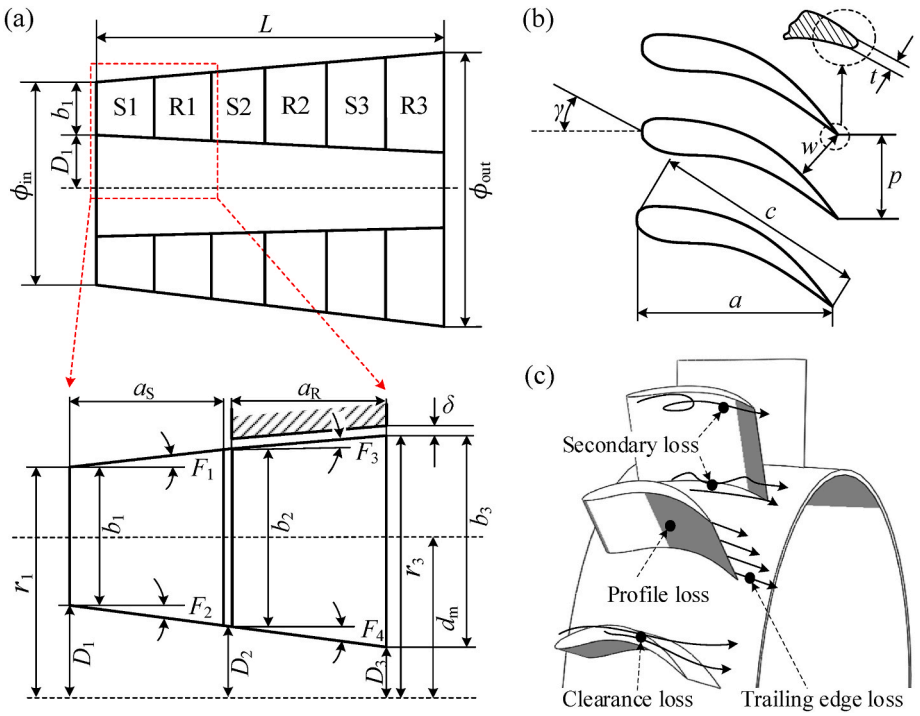

Fig. 5. Geometrical parameters for turbine blades. (a) The three-stages design. (b) The characteristic sizes of turbine blade. (c) Various losses and the corresponding locations. The subfigures of a and b are replotted based on Ref. [32].

Table 1
The operation parameters for sCO_2 coal fired power plant.

Parameters	T1	T2	T3
Inlet temperature (°C)	630.00	630.00	630.00
Inlet pressure (MPa)	35.00	21.10	12.72
Outlet pressure (MPa)	21.31	12.98	7.90
Flow coefficient	0.4		
Load coefficient	0.9		
The degree of reaction	0.5		

3. Based on the Meanline mode [48], λ_2 and δ_R are predicted as

$$\lambda_2 = \sqrt{\frac{1+\lambda_1^2-\frac{\rho_1}{\rho_2}\left(1-\lambda_1^2\right)}{1+\lambda_1^2+\frac{\rho_1}{\rho_2}\left(1-\lambda_1^2\right)}} \tag{27}$$

$$\delta_R = \max\left(5\times10^{-4}d_m, 1\right) \tag{28}$$

The loss in rotor is calculated at various combination sets of geometry parameters for rotor. Again, these parameters shall satisfy the reasonable ranges listed in Table 2. The optimal combination results in the smallest loss in the rotor. The total pressures referring to the relative velocity W_2 (P_{02R}) at node 2 and W_3 (P_{03R}) at node 3, and Y_R are

$$\begin{cases} P_{02R} = f\left(h_2+\frac{W_2^2}{2}, s_2\right), P_{03R} = f\left(h_3+\frac{W_3^2}{2}, s_3\right) \\ Y_R = \frac{P_{02R}-P_{03R}}{P_{03R}-P_3} \end{cases} \tag{29}$$

The internal loop iteration stops once the following criterion is satisfied:

$$\bar{\varepsilon}_{P3} = \left|\frac{P_3-P_3^*}{P_3}\right| \tag{30}$$

Calculations for all the stages of expansion: Similar procedure was performed for all the stages calculation. We note that the parameter λ is optimized for the first stage of turbine. However, for the second stage of turbine, λ_2 can be directly determined based on λ_1, ρ_1 and ρ_2 (see Eq. (27)), hence it is not necessary to optimize λ_2. When the calculation is performed for the last stage (the third stage in this paper), the pressure at node 7 is a given parameter, which is not necessary to be assumed. The loss in the last stage rotor is

$$Y_R = \frac{P_{06R}-P_{07R}^*}{P_{07R}^*-P_7} \tag{31}$$

The total-to-total turbine efficiency is predicted by Eq. (6). If the following criterion

$$\bar{\varepsilon}_\eta = \left|\frac{\eta_{tt}-\eta_{tt}^*}{\eta_{tt}}\right| \le 0.0001 \tag{32}$$

satisfies, the whole computation stops. Otherwise, using the newly obtained η_{tt} to repeat the above procedure. Three key overall sizes of the turbine are determined by

Table 2
The constraint condition for axial turbines.

Geometry parameter	minimum value	maximum value
λ_1	0.30	0.95
λ_3	0.30	1.00
F_S (°)	0.00	20.00
F_R (°)	0.00	25.00
$(b/d_m)_3$	0.00	0.25
$\arcsin(w/s)_S$ (°)	13.00	60.00
$\arcsin(w/s)_R$ (°)	13.00	60.00
$(a/d_m)_S$	0.00	0.25
$(a/d_m)_R$	0.00	0.25
a_S (mm)	3.00	100.00
a_R (mm)	3.00	100.00
w_S (mm)	1.50	100.00
w_R (mm)	1.50	100.00
z_S	10	100
z_R	10	100

Table 3
Comparison of turbine design results with Ref. [9].

Parameter	Ref. [9]	Present study	Relative error (%)
Inlet blade span (mm)	14.60	15.20	4.11
Inlet hub radius (mm)	135.70	134.80	0.66
Outlet blade span (mm)	17.30	17.90	3.46
Outlet hub radius (mm)	134.20	133.50	0.52
isentropic efficiency (%)	84.86	85.57	0.83

Table 4
Comparison of turbine design results with Ref. [53].

Parameter	Ref. [53]	Present study	Relative error (%)
d_m of stage 1 (mm)	106.05	100.66	5.08
d_m of stage 2 (mm)	112.67	109.98	2.38
d_m of stage 3 (mm)	124.51	119.38	4.12
a of stage 1 stator (mm)	20.00	19.13	4.35
a of stage 2 stator (mm)	22.00	23.04	4.72
a of stage 3 stator (mm)	24.00	24.88	3.67
a of stage 1 rotor (mm)	17.00	15.79	7.11
a of stage 2 rotor (mm)	18.00	19.41	7.83
a of stage 3 rotor (mm)	20.00	22.20	11.00
b of stage 1 stator (mm)	25.88	24.79	4.21
b of stage 2 stator (mm)	23.62	24.55	3.93
b of stage 3 stator (mm)	23.19	24.11	3.97
b of stage 1 rotor (mm)	41.05	38.95	5.12
b of stage 2 rotor (mm)	35.15	36.41	3.56
b of stage 3 rotor (mm)	32.26	34.78	7.81
total-total efficiency (%)	91.60	93.85	2.45

$$\phi_{in} = 2(b_1 + D_1), \phi_{out} = 2(b_7 + D_7), L = 1.8\sum_{i=1}^{3} a_i \tag{33}$$

3.3. The loss model for axial flow turbines

Typical losses for axial turbines are shown in Fig. 5c, including profile loss (Y_p), secondary loss (Y_s), clearance loss (Y_{cl}), and trailing edge loss (Y_{te}). Reasonable estimate of these losses is important to predict turbine efficiency. Various models for these losses exist in the literature, including AM model [49], ADMC model [50], C&Cox model [51], Balje model [52], KO model [40], and Aungier model [44]. Detailed comments on these models are beyond the scope of this paper, but the Aungier model [44] was used here. This is because the Aungier model [44] was established on the basis of the AM model [49] and AMDC model [50] and referenced to the KO model [40]. Hence, the Aungier model [44] has improved prediction accuracy than other models. Besides, the Aungier model [44] introduces additional losses due to vibration and high Mach number flow. Because the Aungier model [44] established strong connections between clearance loss and trailing edge loss with geometry parameters of turbines, the model is suitable for sCO_2 turbines. The losses for stator and rotor are

$$Y_S = Y_p + Y_s + Y_{te}, Y_R = Y_p + Y_s + Y_{cl} + Y_{te} \tag{34}$$

Where the subscripts S and R stand for stator and rotor, respectively. The Y_p is [44].

$$Y_p = k_{mod}k_{inc}k_p k_{Re}\left(\left(Y_{p1} + \xi^2\left(Y_{p2} - Y_{p1}\right)\right)\left(\frac{5t_{max}}{c}\right)^{|\xi|} - \Delta Y_{te}\right) \tag{35}$$

Where Y_{p1} and Y_{p2} are profile losses due to nozzle blades and impulse blades, respectively, $\xi = \alpha_1/\alpha_2$ is the ratio of flow angles, k_{mod} is the design technology factor, setting as 0.67, k_{inc} is the off-design factor, which is 1 for steady operation, k_p is the Mach number factor to consider the profile loss, k_{Re} is the Reynolds number factor, t_{max} is the maximum blade thickness, ΔY_{te} is the additional trailing edge loss in the Aungier model [44]. The Y_s is [44]

$$Y_s = k_{Re}k_s\sqrt{\frac{\widetilde{Y}_s^2}{1 + 7.5\widetilde{Y}_s^2}} \tag{36}$$

$$\widetilde{Y}_s = 0.0334F_{AR}Z\frac{\cos\alpha_2}{\cos\gamma} \tag{37}$$

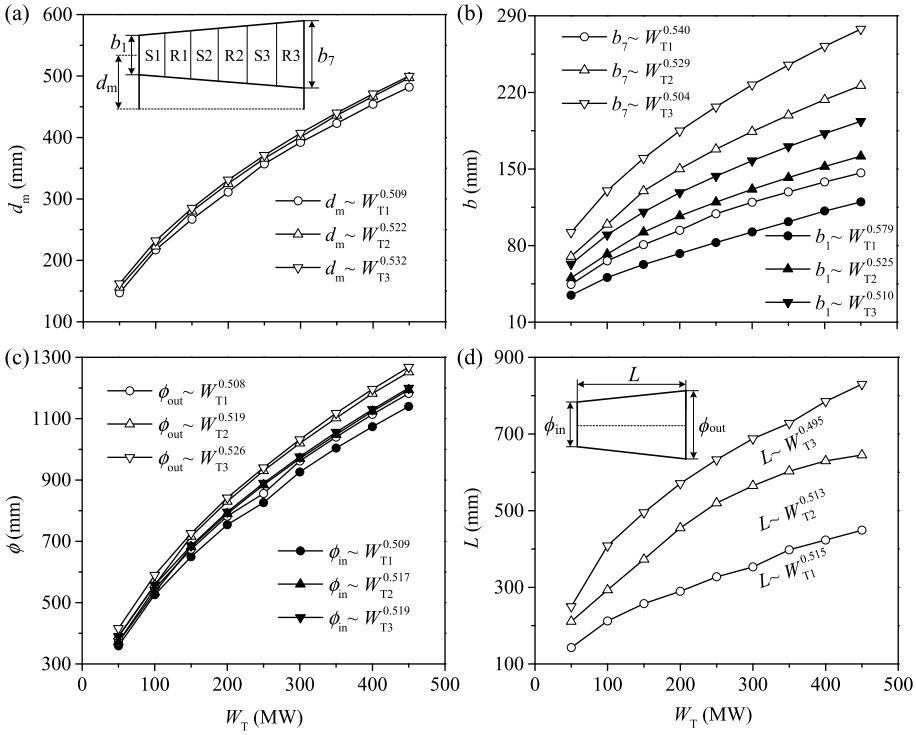

Fig. 6. Overall turbine sizes dependent on power capacities for three turbines of T1, T2 and T3. (a) d_m versus W_T, (b) b versus W_T, (c) ϕ versus W_T, and (d) L versus W_T.

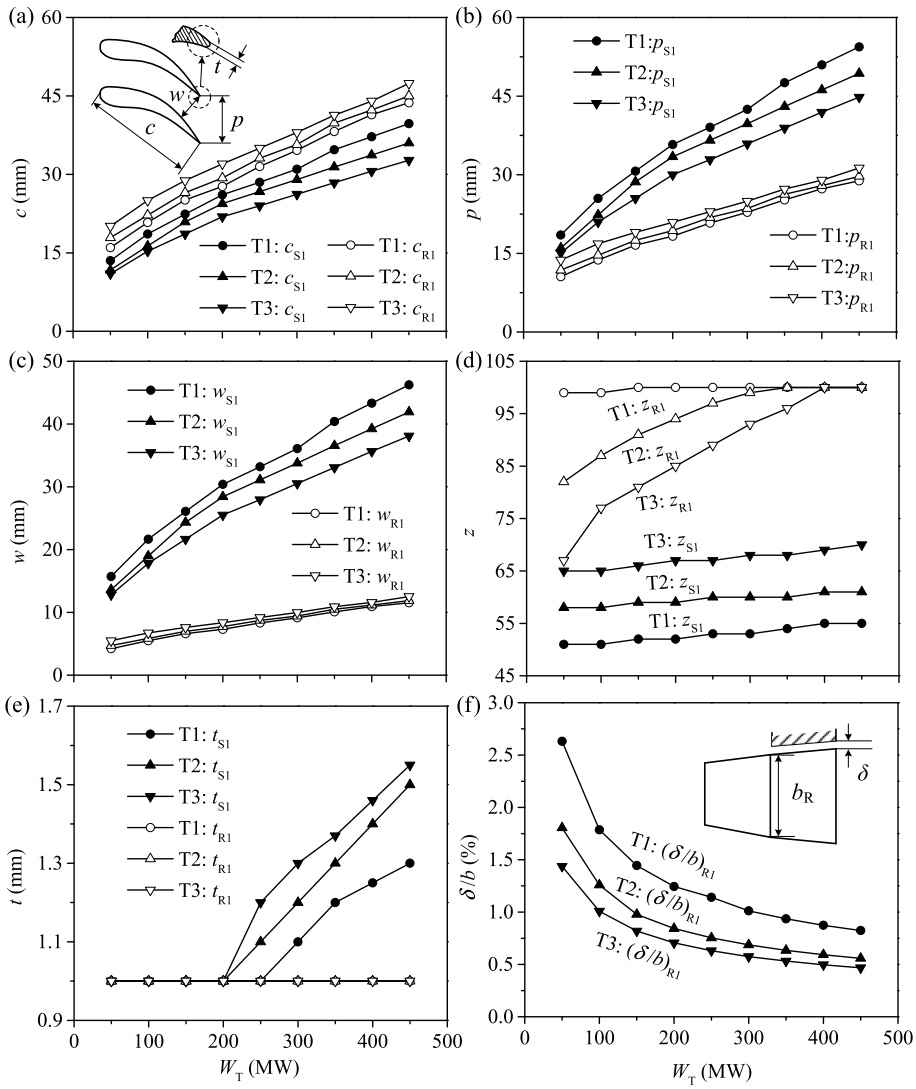

Fig. 7. Characteristic turbine sizes dependent on power capacities for three turbines of T1, T2 and T3. (a) c versus W_T, (b) p versus W_T, (c) w versus W_T, and (d) z versus W_T, (e) t versus W_T, (f) δ/b versus W_T.

$$Z = \left(C_L \frac{c}{p}\right)^2 \frac{\cos^2\alpha_2}{\cos^3\alpha_m} \tag{38}$$

$$C_L = 2|\tan\alpha_2 - \tan\alpha_1|\frac{p}{c}\cos\alpha_m \tag{39}$$

Where $\widetilde{Y}_s$ is the estimation of the secondary loss, k_s is the Mach number factor considering secondary loss, F_{AR} is the factor considering effects of blade height and chord length, Z is the Ainley loading parameter, α_m is the average flow angle. For first stage, α_m is $90^o - \arctan((\cot\alpha_1 - \cot\alpha_2)/2)$ for stator, and $90^o - \arctan((\cot\beta_2 - \cot\beta_3)/2)$ for rotor, C_L is the lifting coefficient.

The clearance loss (Y_{cl}) and trailing edge loss (Y_{te}) are [44].

$$Y_{te} = \left(\frac{t}{w-t}\right)^2 \tag{40}$$

$$Y_{cl} = 0.47Z\frac{c}{b}\left(\frac{\delta}{c}\right)^{0.78} \tag{41}$$

3.4. Validation of the turbine efficiency

Based on the model described in sections 3.1 to 3.3, a numerical code is developed based on the MATLAB platform. Available studies focus on radial turbines, investigations of axial turbines are seldomly reported. In this paper, a numerical code is developed to predict turbine performance. To verify the correctness of the calculations, we compare our predictions with those reported in Ref. [9]. A two-stages axial turbine is used for a simple sCO_2 cycle driven by the combusting of nature gas [9]. The design parameters are $m = 85$ kg/s, $T_{in} = 600$ °C, $P_{in} = 20$ MPa, $P_{out} = 15.1$ MPa, $n = 10{,}000$ r/min. Under the conditions of $\varphi = 0.4$, $\psi = 0.9$ and $R = 0.45$, the complete 3D numerical simulation gives the turbine efficiency of 84.86% [9]. Table 3 lists the comparison between our calculations with the data in Ref. [9]. We reach the turbine efficiency of 85.57%, well matching the result presented in Ref. [9]. For turbine size estimation, the maximum deviation between our predictions and those of Ref. [9] is smaller than 4.1%. This comparison demonstrates the correctness and effectiveness of our model for sCO_2 axial turbines.

Another comparison was made regarding axial turbine design for solar energy driven sCO_2 cycle. The design parameters involve $W_T = 10$ MW, $T_{in} = 500$ °C, $P_{in} = 15$ MPa, $P_{out} = 9.5$ MPa and $n = 10{,}000$ r/min [53]. Axial turbine is used with $R = 0.1$, 0.15, 0.18 respectively for the three stages expansion. They used the flow angles of α and β instead of using φ and ψ, and used the speed coefficient to replace the loss models. These treatments simplify the calculation procedure. It is noted that the average diameters for the three stages blade are different. To make a direct comparison between our outcomes and the data reported in

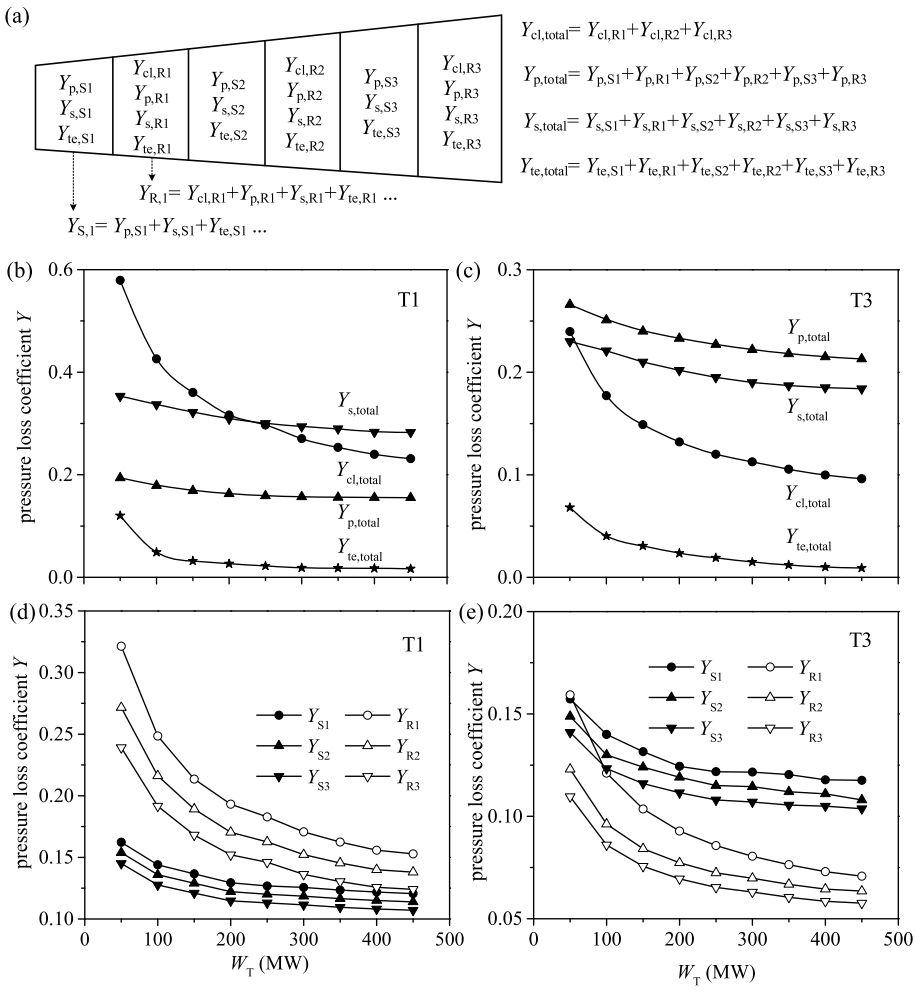

Fig. 8. Various losses in turbines T1 and T3. (a) The distribution of losses in stator and rotor of the three-stages turbine, (b) the four losses summarized across the whole turbine T1, (c) the four losses summarized across the whole turbine T3, (d) the losses in stator and rotor of the three-stages turbine T1, (e) the losses in stator and rotor of the three-stages turbine.

Ref. [53], our model is reasonably modified to adapt their situations. Table 4 shows that regarding the turbine geometry dimensions, the maximum deviation between our results and those given in Ref. [53] is less than 5%. Regarding the turbine efficiency, Ref. [53] gave the value of 85% by using their simplified model. Their 3D numerical simulation gave the turbine efficiency of 93.8%, approaching the value of 91.6% for the present prediction. The above comparisons indicate that the model presented in this paper has sufficient accuracy to predict the sizes and efficiencies for axial turbines of sCO_2.

Here, we emphasize that the determination of turbine efficiencies in different power capacities is an important issue, which guides the design and optimization of sCO_2 power cycles. The turbine efficiency can be determined based on the three-dimensional computation-fluid -dynamics (CFD) simulation. This work provides a simple but accurate model for the analysis of sCO_2 turbines, which is cost-effective. It is also noted that the present work focusses on the analysis of axial turbines. The turbine efficiencies for small power capacity should be conducted in the future. Under such circumstance, the centrifugal turbines are needed.

4. Results and discussion

4.1. Scaling law of geometric sizes with respect to power capacities

We theoretically developed the scaling laws of geometry sizes dependent on power capacities. Eq. (7) indicates $m \sim W_T$. Combining Eqs. (7) and (20), one reaches the passage area at entrance location $A_1 \sim W_T$. Further combining Eqs. (7), (20) and (21) yields the scaling law of $d_m \sim W_T^{1/2}$, where d_m is the average diameter. Simple deduction yields similar scaling law of $l_c \sim W_T^{1/2}$. Here, l_c is the characteristic length of axial turbines, which can be average diameter (d_m), blade height (b), hub radius (D), overall diameters at inlet and outlet (φ_{in} and φ_{out}) and overall length (L).

Fig. 6 shows the sizes of d_m, b_1, b_7, ϕ_{in}, ϕ_{out} and L versus W_T. Based on numerical simulations, curve fittings yield the following scaling laws

$$\begin{cases} d_m \sim W_T^{0.509\sim0.532}, b \sim W_T^{0.504\sim0.551} \\ \phi \sim W_T^{0.508\sim0.526}, L \sim W_T^{0.495\sim0.515} \end{cases} \quad (42)$$

It is seen that Eq. (42) perfectly agrees with the scaling law of $l_c \sim W_T^{1/2}$. It is noted that our calculations are performed for three turbines of T1, T2 and T3, which have different P_{in}, T_{in} and P_{out} (see Table 1). The mini deviation of the power exponent from 0.5 is due to different P_{in}, T_{in} and P_{out} used for the three turbines, and expansion induced losses for each turbine. Basically, the flow passage area A_1 is directly proportional to W_T. Because the expansion process displays the similarity characteristic at various power capacities, the relationship between l_c and A_1 yields $l_c \sim A_1^{0.5}$, yielding $l_c \sim W_T^{1/2}$.

Further verification of the scaling law includes chord length c, pitch distance p and blade throat w (see Fig. 7a–c). Curve fittings give the following correlations:

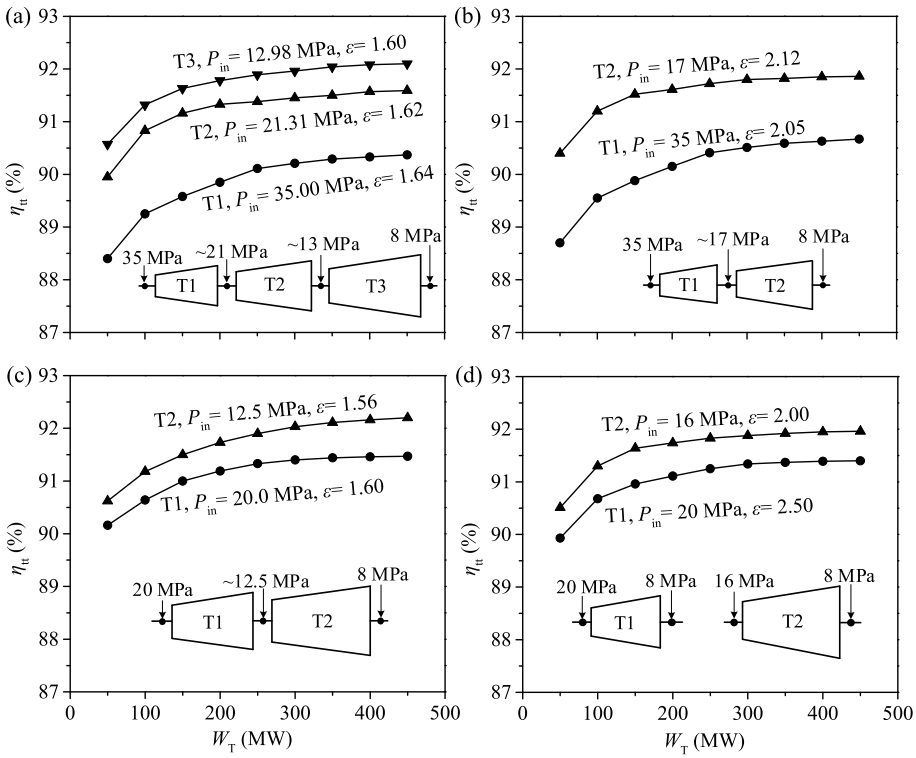

Fig. 9. Turbine efficiencies dependent on power capacities. (a) Efficiencies for three turbines applied for sCO_2 coal fired power plant with double-reheating. (b) Efficiencies for two turbines applied for sCO_2 coal fired power plant with reheating. (c) Efficiencies for two turbines applied for solar/nuclear energies driven sCO_2 cycles with reheating. (d) Efficiencies for independent turbines at 16 or 20 MPa pressure level.

$$c \sim W_T^{0.479\sim0.518}, p \sim W_T^{0.479\sim0.518}, w \sim W_T^{0.479\sim0.518} \tag{43}$$

In Fig. 7a-c, the subscripts S1 and R1 represent stator and rotor for the first stage expansion, respectively, indicating significantly different c, p and w for stator and rotor. Compared with stator, rotor needs larger chord length, but has much smaller pitch and blade throat. Fig. 7d–f shows the number of blades (z), trailing edge thickness (t), and relative clearance (δ/b). Rotor has larger number of blades than stator. The z for rotor increases with increases of W_T, but slightly increases with increase of W_T for stator. For T1, an exception exists that z keeps a constant of 100, which is due to the maximum limit setting in this paper (see Fig. 7d). Too many rotor blades would cause fluid blockage to deteriorate performance. On the contrary, the minimum criterion of t is encountered with $W_T < 200$ MW for all the three turbines (see Fig. 7e). The relative clearance decreases with increase of power capacities (see Fig. 7f), indicating narrowed nuzzle expansion for larger power generation. Because sCO_2 turbines operate at pressures higher than the critical pressure, the expansion process takes place at high fluid densities, ensuring much compact geometry sizes, compared with water-steam or organic fluids turbines [54].

4.2. Various losses dependent on power capacities

Eqs. (35), (36), (40) and (41) give expressions for various losses of turbines. Let us examine how the profile loss Y_p varies versus W_T first. In Eq. (35), k_{mod} and k_{inc} are not dependent on W_T. The k_p is the Mach number factor, not influenced by W_T. Then, Eq. (35) becomes

$$Y_p \sim k_{Re} \times \left(\left(Y_{p1} + \xi^2 \left(Y_{p2} - Y_{p1}\right)\right) \left(\frac{5t_{max}}{c}\right)^{|\xi|} - Y_{te} \right) \tag{44}$$

In Eq. (44), Y_{p1} and Y_{p2} are correlated with flow angles of α and β [44]. The ratio of flow angles ξ is also not dependent on power capacities. The t_{max} is set as 0.2c [44]. The term of Y_{te} has smaller contribution than Y_{p1} and Y_{p2}. The above analysis yields the scaling law of $Y_p \sim k_{Re}$. Because k_{Re} is [44]

$$k_{Re} = \left(\log_{10}\left(5 \times 10^5\right)\right)^{1.25} \times Re^{-0.15} \quad \text{for } Re > 5 \times 10^5 \tag{45}$$

Considering $Re \sim d_m \sim W_T^{0.5}$ yields the scaling law of $Y_p \sim W_T^{-0.075}$.

Similar deduction yields the scaling laws of the four losses with respect to power capacities as

$$\begin{cases} Y_p \sim W_T^{-0.075}, Y_s \sim W_T^{-0.075} \\ Y_{cl} \sim W_T^{-0.390}, Y_{te} \sim W_T^{-1.000} \end{cases} \tag{46}$$

Eq. (46) indicates that profile loss Y_p and secondary loss Y_s decrease versus W_T according to the power law of −0.075, but the clearance loss Y_{cl} and trailing edge loss Y_{te} decrease versus W_T according to the power law of −0.39 and −1, respectively.

To verify the correctness of Eq. (46), various losses are summarized in Fig. 8a. In Fig. 8b–e, the subscript "total" means total loss integrated across the whole three-stages turbine, p, s, cl and te represent profile loss, secondary loss, clearance loss and trailing edge loss, respectively. The subscripts S and R stand for stator and rotor, respectively. Fig. 8b–c indicates that the four terms of losses decrease versus W_T. Curve fitting of the four losses yields the scaling law as

$$\begin{cases} Y_p \sim W_T^{-0.077\sim-0.074}, Y_s \sim W_T^{-0.081\sim-0.072} \\ Y_{cl} \sim W_T^{-0.409\sim-0.387}, Y_{te} \sim W_T^{-1.007\sim-0.912} \end{cases} \tag{47}$$

Eqs. (46) and (47) are in good agreement with each other, noting that the above scaling laws are suitable for both T1 and T3. Remember that the profile loss Y_p is caused by the skin friction between fluid and solid wall, and the secondary loss Y_s is caused by the generation of vortex [44]. These two losses decrease when the turbulent intensity increases. The Reynolds number (Re) increases with increase of power capacities, decreasing the skin friction and vortex effect. This explains why Y_p and Y_s decrease with increases of turbine powers. The clearance loss Y_{cl}

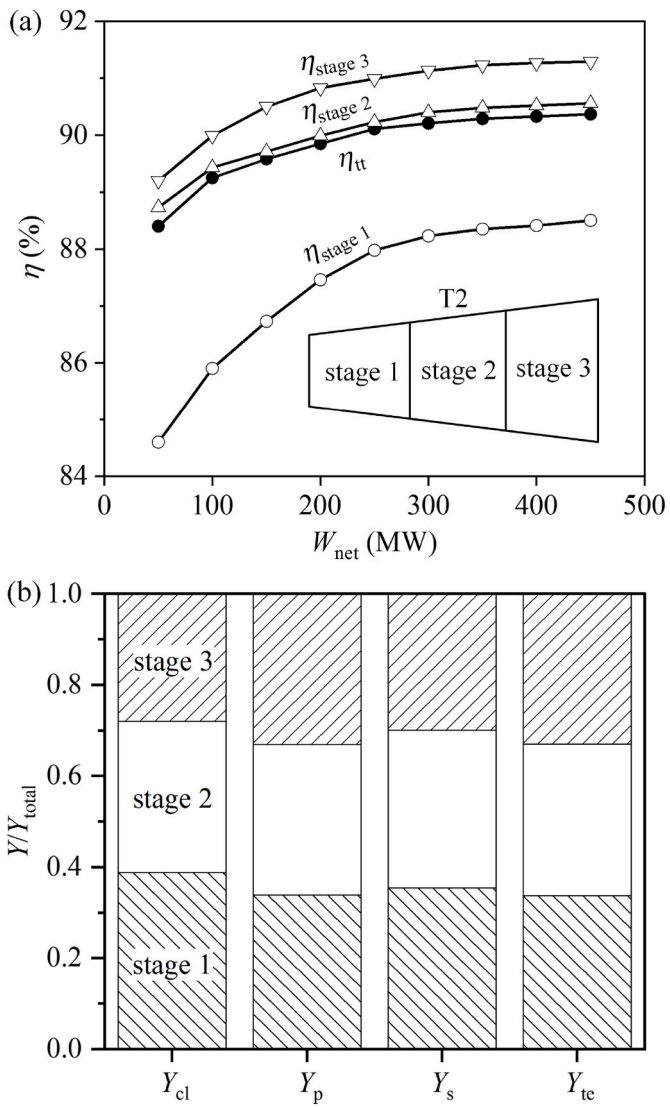

Fig. 10. Efficiencies for the three stages of T2 (a) and the contributions of various losses in the three stages of T2 (b).

represents the leakage effect, which becomes weak when increasing power capacities. The trailing edge loss Y_{te} is caused by the mixing of the trailing flow and the main streamline flow. When W_T (or say turbine size) increases, the mixing induced blockage becomes weak to decrease Y_{te}.

The high-pressure turbine T1 has larger losses than the low-pressure turbine T3, which is due to the higher density fluid expansion due to higher pressure operating (see Fig. 8b–c). The operating pressures also influence the relative magnitudes of losses in stator and rotor. For T1, rotor contributes larger losses than stator (see Fig. 8d). On the contrary, losses in stator become more important than rotor for T3 (see Fig. 8e).

4.3. Turbine efficiencies dependent on power capacities

The number of turbines is related to cycle configuration. If one uses double-reheating, three turbines T1, T2 and T3 are used (see Fig. 1). Pressures consecutively decrease from T1 to T3. Turbine efficiencies η_{tt} are plotted versus power capacities in Fig. 9a. The low-pressure turbine T3 and high-pressure turbine T1 have the largest and smallest efficiencies respectively to indicate the pressure effect. The η_{tt} is small at $W_T = 50$ MW, quickly increases with increase of W_T but with decreased slope of the efficiency curves for $W_T > 300$ MW. The performance of small capacity turbine agrees with those reported in the literature, for which η_{tt} is usually smaller than 90% [9,55].

Only two turbines T1 and T2 are necessary adapting to reheating instead of double-reheating for coal fired power plant. Comparing Fig. 9a and b, the expansion pressure ratio, which is defined as $\epsilon = P_{in}/P_{out}$ for each turbine, becomes larger when using two turbines instead of three. Both Fig. 9a and b shows similar curve trend of efficiencies, but T3 in Fig. 9a has larger efficiencies than T2 in Fig. 9b, majorly caused by the lower operating pressure for T3.

Attention is also paid to solar energy or nuclear energy driven sCO_2 cycle, involving narrow temperature range of heat carrier fluid coupling with cycle [1]. Because the temperature difference of the heat carrier fluid entering the cycle and leaving the cycle is small, recompression cycle (RC) can be applied. Coupling reheating and RC needs two turbines. The operating pressures can be lower than the coal fired cycle applications. Again, the efficiency curves in Fig. 9c show similar trend as Fig. 9a–b. However, T1 in Fig. 9c has elevated efficiencies than T1 in Fig. 9a, due to the pressure effect. We note that Fig. 9a–c are for two or three turbines working with consecutive decrease of pressures. Independent turbines are considered in Fig. 9d. Because P_{out} is usually set as a value such as 8 MPa, which is slightly higher than the critical pressure [5], the two curves in Fig. 9d represent $P_{in} = 16$ MPa ($\epsilon = 2.0$) and 20 MPa ($\epsilon = 2.5$), respectively.

We note that each turbine contains three stages. One may be interested to the efficiencies for each stage of the turbine. The efficiencies are plotted in Fig. 10a for the three stages of turbine T2, showing the smallest efficiencies for the first stage and largest efficiencies for the third stage. During expansion of the fluid in the turbine, the first stage has largest surface area to the volume ratio for the expansion channel, hence the losses in the first stage are the largest to have smallest efficiencies. This conclusion is verified by Fig. 10b, noting that Y_{total} is the total losses in T2. The Y_{total} is decoupled into Y_{cl}, Y_p, Y_s and Y_{te}. Among them, Y_p and Y_{te} have similar contributions for all the three stages. The stage 1 has the largest contributions of Y_{cl} and Y_s, but the stage 3 has the smallest contributions of Y_{cl} and Y_s. The data presented in Fig. 10b supports the results shown in Fig. 10a.

4.4. Turbine efficiencies dependent on pressure ratio, temperature and pressure level

The expansion pressure ratio (ϵ) is important to influence turbine performance. The η_{tt} has parabola distribution with respect to ϵ for $W_T = 450$ MW and 50 MW (see Fig. 11a). The peak efficiency takes place at $\epsilon = 2$. This trend is related to the relative magnitudes of various losses in turbines (see Fig. 11b for $W_T = 50$ MW case). For rotor, pressure loss coefficients in the three stages of rotor (Y_{R1}, Y_{R2} and Y_{R3}) are almost flat with $1.55 < \epsilon < 2.0$, but the increase slopes become larger for ϵ beyond of 2.0. Meanwhile, pressure loss coefficients in the three stages of stator show decrease, minimum followed by increase (parabola curve), indicating different responses of losses to the variation of ϵ for rotor and stator. The total pressure drop across the whole turbine is recorded as ΔP_{total}, including six components in the three stages of stator and rotor (see Fig. 11c). Definitely, ΔP_{total} equals to $P_{in}(1\text{-}1/\epsilon)$. To explain the parabola distribution of turbine efficiencies, each pressure drop in the three stages of stator and rotor is decoupled into a part for useful thermal-power conversion, and a part for irreversibility loss (dispersion). Thus, the irreversible pressure drop (dispersion) for stator and rotor are

$$\Delta P_{S,loss} = \sum_{i=1}^{3} Y_{S,i}\Delta P_{S,i}, \Delta P_{R,loss} = \sum_{i=1}^{3} Y_{R,i}\Delta P_{R,i} \quad (48)$$

Where the subscripts S, R, i refer to stator, rotor and the ith stage expansion, respectively. In Fig. 11d, $\Delta P_{S,loss}/\Delta P_{total}$, $\Delta P_{R,loss}/\Delta P_{total}$ and $(\Delta P_{S,loss} + \Delta P_{R,loss})/\Delta P_{total}$ quantify the irreversible degree in stator, rotor, and both stator and rotor relative to total pressure drop. The

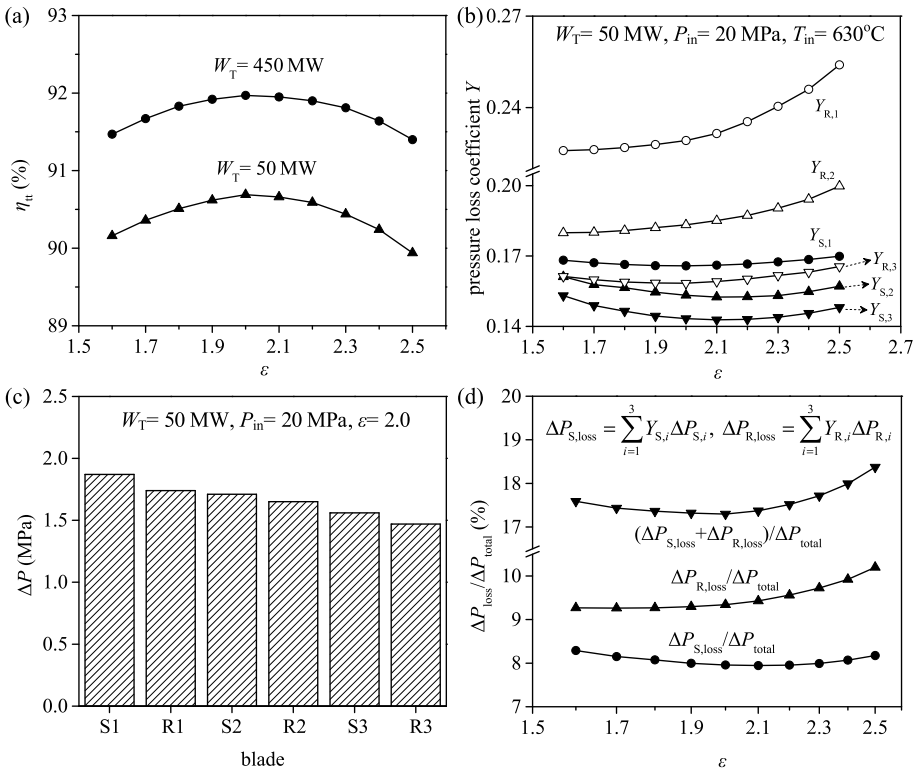

Fig. 11. Effect of expansion pressure ratio on turbine efficiencies. (a) The parabola distribution of η_{tt} with respect to ε. (b) Loss coefficient for each stage stator and rotor. (c) Pressure drops along the axial expansion direction. (d) Pressure drops in stator and rotor dependent on expansion pressure ratio.

irreversible pressure loss including stator and rotor displays the parabola distribution versus the expansion pressure ratio, attaining minimum at $\epsilon = 2$. The irreversible loss curve shown in Fig. 11d successfully explains the turbine performance curve shown in Fig. 11a. The sCO_2 turbines achieve maximum efficiency when the expansion pressure ratio approaches 2, at which the irreversible loss gets minimum.

The above outcomes are presented for $T_{in} = 630$ °C. Effects of P_{in} and T_{in} on turbine efficiencies are shown in Fig. 12. The efficiency map is presented for three turbine powers of 450 MW, 250 MW and 50 MW, representing larger-scale, moderate-scale and small-scale utilizations. The distribution of these curves shows similar trends for different power capacities. Turbine efficiencies are more sensitive to pressures than temperatures. The η_{tt} decreases with increases of pressures. By fixing W_T, the increase of pressures results in the rise of CO_2 densities. This effect directly decreases flow velocities to ensure the Reynolds number (Re) becoming smaller. Hence, the skin friction increases and the vortex intensity becomes larger. Correspondingly, various losses such as the profile loss (Y_p) and the secondary loss (Y_s) increase to deteriorate turbine efficiencies at higher pressures.

Compared with the effect of pressures, the effect of temperatures is weak. The general trend is that turbine efficiencies slightly decrease with increase of T_{in}. This finding is logically explained here. The increase of T_{in} increases the enthalpy difference between inlet and outlet (Δh). By fixing W_T, this effect decreases the mass flow rate, based on $W_T = m\Delta h$. Hence, the Reynolds number decreases to increase the irreversible losses such as Y_p and Y_s.

We conclude that turbine efficiency is slightly deteriorated when increasing inlet fluid temperature, by fixing the turbine power. Our finding is not contradictory to the conclusion drawn in the literature [56]. In most of references [47,49], the conclusion "turbine efficiency becomes better when using higher inlet fluid temperature" was drawn by fixing the mass flow rate. Based on the Clapeyron Equation $P = \rho RT$, the increase of T decrease ρ. Then, based on $m = \rho VA$, this effect increases the flow velocity to increase the Re. Hence, various losses decrease to elevate the turbine efficiency when increasing T_{in} at given mass flow rate. In summary, our finding regarding the inlet temperature effect and those drawn in the literature are based on different conditions. The former was based on constant turbine power and the later was based on constant mass flow rate.

4.5. Comments on the turbine efficiencies dependent on power capacities

As a common technology, sCO_2 cycle can be applied driven by various heat sources. For coal fired power plant, one not only pursues higher cycle efficiency, but also expects higher flexibility to balance dynamic load variations of renewable energies. For these applications, the sCO_2 power plant may cover a wide range of power capacities in the range of (100–1000) MWe. For solar energy driven sCO_2 cycle, the power capacity may be (50–100) MWe. Here, we investigate turbine efficiencies dependent on power capacities. The results can be integrated in the cycle analysis. Thus, reliable prediction of the whole cycle performance would be reached. Together with future investigations, the present work is helpful to select and judge specific power capacity of power plant as well as turbine itself, which could have comprehensive performance in efficiency, cost, and flexibility degree.

Our model has acceptable accuracy in prediction of turbine efficiency and characteristic size. In section 3.4, we compare our results with those reported in the literature. It is shown that the predicted turbine efficiency can be comparable with those predicted by the 3D numerical simulations. Thus, the present model is efficient and accurate for the prediction of turbine performance. Our work indicates the scaling laws regarding the characteristic sizes as $l_c \sim W_T^{0.5}$ shown in Eqs.(42) and (43), and the four types of losses shown in Eqs.(46) and (47). These scaling laws helps us understand how these parameters are influenced by the power capacities of turbines. These scaling laws are not mentioned in the literature. We further compared our scaling law results with the data reported in the literature. Ref. [57] investigated three-stage axial turbine with W_T in the range of (3∼300) MW and inlet

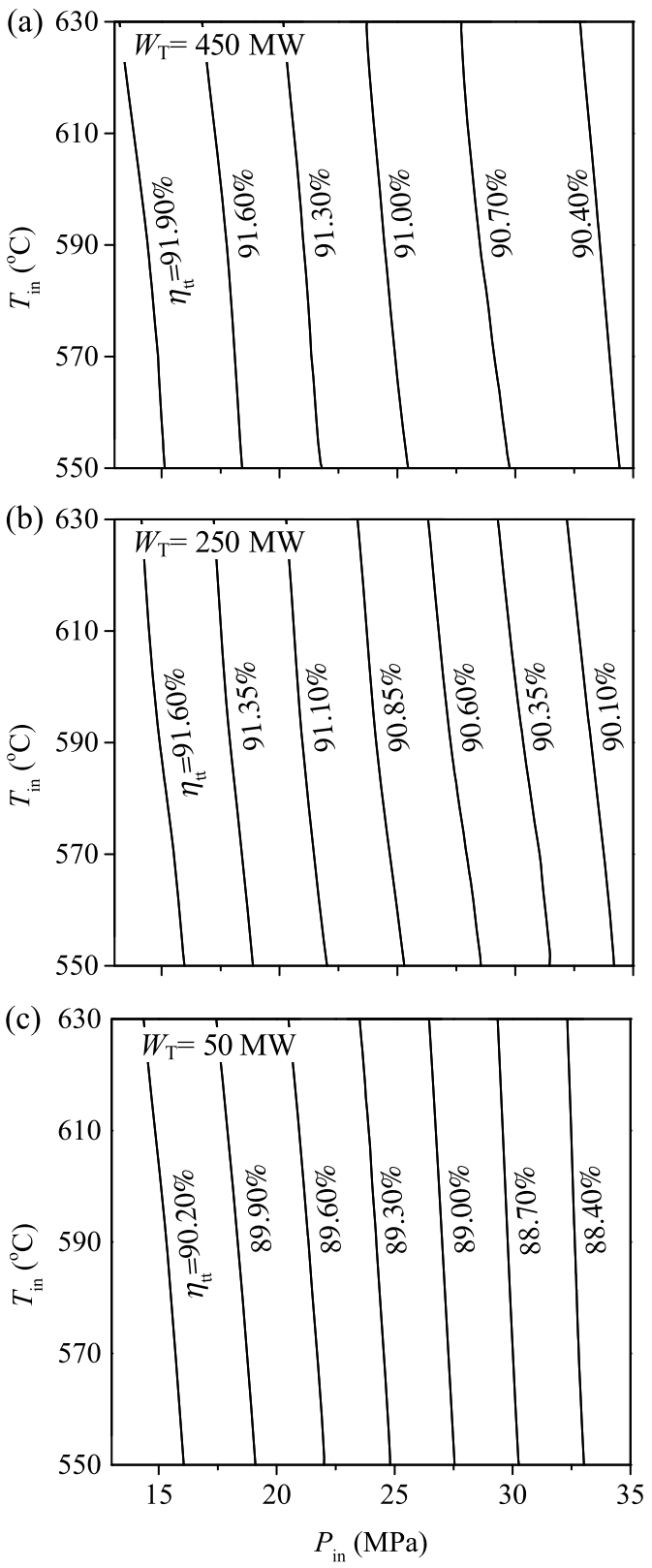

Fig. 12. Effect of inlet pressures and temperatures on turbine efficiencies at the expansion pressure ratio of 1.6. (a) 450 MW capacity, (b) 250 MW capacity, (c) 50 MW capacity.

and outlet pressures of 20 MPa and 7.7 MPa, respectively. They plotted outer diameters of turbines (φ) versus power capacities of the turbines (see Fig. 4 in Ref. [57]). The curve fitting by the present authors using their data gives $\phi \sim W_T^{0.487\sim0.498}$, satisfying the scaling law proposed in this paper. Another verification of the scaling law is given here. Ref. [58] investigated single-stage axial turbine. The design parameters are T_{in} = 565 °C, P_{in} = 20 MPa, and P_{out} = 8 MPa. They gave the normalized blade height b and chord length c versus power capacities of turbines in Fig. 11 of Ref. [58]. The curving fitting by the present authors using their data gave $b \sim W_T^{0.481}$ and $c \sim W_T^{0.513}$ with W_T in the range of (10~50) MW, also satisfying the scaling law presented in this paper.

In the end of this paper, we give a short comment on the effect of inlet fluid temperatures (T_{in}). One notes that the turbine efficiency and cycle efficiency are two different terms. The former characterizes the degree of the real expansion process deviating from the isentropic expansion. The latter characterizes how much thermal energy is converted into mechanical power. In this paper, we identify that the effect of T_{in} on turbine efficiency is weak, and the turbine efficiency is slightly decreased with increase of T_{in}. On the other hand, from cycle and system point of view, the increase of T_{in} would decrease the total exergy destructions across the whole system, not just considering the turbine itself. Thus, the system efficiency is increased with increase of T_{in}, which is the highest temperature in the cycle.

5. Conclusions

Conclusions can be drawn as follows.

1. A comprehensive model is presented to predict characteristic sizes, irreversible losses and efficiencies of sCO_2 axial turbines with multi-stages. The calculation results including turbines sizes and efficiencies match the data reported in the literature. The model can be integrated in the cycle analysis for efficient and accurate estimate of turbine performances.
2. Characteristic size of turbines (l_c) obeys the scale law of $l_c \sim W_T^{0.5}$. Profile loss Y_p, secondary loss Y_s, clearance loss Y_{cl} and trailing edge loss Y_{te} obey the scale laws of $Y_p \sim W_T^{-0.075}$, $Y_s \sim W_T^{-0.075}$, $Y_{cl} \sim W_T^{-0.39}$, $Y_{te} \sim W_T^{-1}$. These scaling laws agree with the correlations based on numerical simulations.
3. Turbine efficiencies are presented dependent on power capacities. With W_T increase from 50 MW to 450 MW, turbine efficiencies quickly increase first and then the slope of the curves decreases. This variation trend is due to the decreased irreversible losses when W_T increases.
4. Turbine efficiencies show parabolic variation with respect to expansion pressure ratios. The efficiencies get maximum when the expansion pressure ratio equals to 2, at which the irreversible loss reaches minimum.
5. Efficiency maps are presented based on inlet pressure P_{in} and temperature T_{in}. By fixing the turbine power, the η_{tt} decreases with increase of P_{in}. Under such circumstance, the irreversible losses increase due to the decreased Reynolds number. The η_{tt} is insensitive to the variation of T_{in}.

Credit author statement

Tianze Wang: Methodology, Software, Investigation, Writing –original draft. **Jinliang Xu:** Conceptualization, Methodology, Funding acquisition, Writing –review & editing. **Zhaofu Wang:** Conceptualization, Supervision, Writing –review & editing. **Haonan Zheng:** Methodology, Validation. **Jianhui Qi:** Methodology, Validation. **Guanglin Liu:** Formal analysis.

Declaration of competing interest

The authors declare that they have no known competing financial interests or personal relationships that could have appeared to influence the work reported in this paper.

Data availability

Data will be made available on request.

Acknowledgements

This work was supported by the Natural Science Foundation of China (52130608, 51821004).

References

[1] Li M, Zhu H, Guo J, Wang K, Tao W. The development technology and applications of supercritical CO_2 power cycle in nuclear energy, solar energy and other energy industries. Appl Therm Eng 2017;126:255–75.
[2] Wang K, He Y, Zhu H. Integration between supercritical CO_2 Brayton cycles and molten salt solar power towers: a review and a comprehensive comparison of different cycle layouts. Appl Energy 2017;195:819–36.
[3] Guo Z, Zhao Y, Zhu Y, Niu F, Lu D. Optimal design of supercritical CO_2 power cycle for next generation nuclear power conversion systems. Prog Nucl Energy 2018;108:111–21.
[4] Song J, Li X, Ren X, Gu C. Performance improvement of a preheating supercritical CO_2 cycle based system for engine waste heat recovery. Energy Convers Manag 2018;161:225–33.
[5] Xu J, Liu C, Sun E, Xie J, Li M, Yang Y, et al. Perspective of sCO_2 power cycles. Energy 2019;186:115831.
[6] Moore J, Day M, Cich S, Hofer D, Mortzheim J. Testing of a 10 MWe supercritical CO_2 turbine. In: Proceedings of the 47th turbomachinery symposium. Turbomachinery Laboratory, Texas A&M Engineering Experiment Station; 2018. p. 17–20. September.
[7] Wright SA, Radel RF, Vernon ME, Rochau GE, Pickard PS. Operation and analysis of a supercritical CO_2 Brayton cycle. Albuquerque: Sandia National Laboratories; 2010. SAND2010-0171.
[8] Cho J, Shin H, Cho J, Ra HS, Roh C, Lee B, et al. Preliminary power generating operation of the supercritical carbon dioxide power cycle experimental test loop. In: The 6th international supercritical CO_2 power cycles symposium, Pennsylvania, USA; 2018. p. 27–9. march.
[9] Han W, Feng Z, Wang Y, Li H, Zhou D, Dan G, et al. Aerodynamic design and performance of S-CO_2 high pressure turbines. J Harbin Inst Technol 2018;50(7):192–8 [in Chinese].
[10] Angelino G. Real gas effects in carbon dioxide cycles. In: ASME 1969 gas turbine conference and products show. American Society of Mechanical Engineers; 1969. V001T01A071-V001T01A071.
[11] Bidkar RA, Mann A, Singh R, Sevincer E, Cich S, Day M. Conceptual designs of 50 MWe and 450 MWe supercritical CO_2 turbomachinery trains for power generation from coal. Part 1: cycle and turbine. In: The 5th symposium-supercritical CO_2 power cycles, Texas, USA; 2016. p. 28–31. march.
[12] Li H, Zhang Y, Yao M, Yang Y, Han W, Bai W. Design assessment of a 5 MW fossil-fired supercritical CO_2 power cycle pilot loop. Energy 2019;174:792–804.
[13] Qi J, Reddell T, Qin K, Hooman K, Jahn IH. Supercritical CO_2 radial turbine design performance as a function of turbine size parameters. J Turbomach 2017;139(8):081008.
[14] Zhou A, Song J, Li X, Ren X, Gu C. Aerodynamic design and numerical analysis of a radial inflow turbine for the supercritical carbon dioxide Brayton cycle. Appl Therm Eng 2018;132:245–55.
[15] Lee S, Yaganegi G, Mee DJ, Guan Z, Gurgenci H. Part-load performance prediction model for supercritical CO_2 radial inflow turbines. Energy Convers Manag 2021;235:113964.
[16] Utamura M, Hasuike H, Ogawa K, Yamamoto T, Fukushima T, Watanabe T, et al. Demonstration of supercritical CO_2 closed regenerative Brayton cycle in a bench scale experiment. In: ASME turbo expo 2012: turbine technical conference and exposition. American Society of Mechanical Engineers; June .
[17] Shin H, Cho J, Baik YJ, Cho J, Roh C, Kang Y, et al. Partial admission, axial impulse type turbine design and partial admission radial turbine test for SCO_2 cycle. In: ASME turbo expo 2017: turbine technical conference and exposition. American Society of Mechanical Engineers; June .
[18] Keep JA, Jahn IHJ. Numerical loss investigation of a small scale, low specific speed supercritical CO_2 radial inflow turbine. J Eng Gas Turbines Power 2019;141(9):091003.
[19] Wang Z, Sun E, Xu J, Liu C, Liu G. Effect of flue gas cooler and overlap energy utilization on supercritical carbon dioxide coal fired power plant. Energy Convers Manag 2021;249:114866.
[20] Muto Y, Aritomi M, Ishizuka T, Watanabe N. Comparison of supercritical CO_2 gas turbine cycle and Brayton CO_2 gas turbine cycle for solar thermal power plants. In: Fourth supercritical CO_2 power cycles symposium, pittsburgh, Pennsylvania; 2014. p. 9–10. September.
[21] Xu J, Sun E, Li M, Liu H, Zhu B. Key issues and solution strategies for supercritical carbon dioxide coal fired power plant. Energy 2018;157:227–46.
[22] Liu C, Xu J, Li M, Wang Z, Xu Z, Xie J. Scale law of sCO_2 coal fired power plants regarding system performance dependent on power capacities. Energy Convers Manag 2020;226:113505.
[23] Fan Y, Tang G, Yang D, Li X, Wang S. Integration of sCO_2 Brayton cycle and coal-fired boiler: thermal-hydraulic analysis and design. Energy Convers Manag 2020;225:113452.
[24] Sun E, Hu H, Li H, Liu C, Xu J. How to construct a combined S-CO_2 cycle for coal fired power plant? Entropy-Switz 2018;21(1):19.
[25] Sun E, Xu J, Hu H, Li M, Miao Z, Yang Y, et al. Overlap energy utilization reaches maximum efficiency for S-CO_2 coal fired power plant: a new principle. Energy Convers Manag 2019;195:99–113.
[26] Li Z, Li Z, Li J, Feng Z. Leakage and rotordynamic characteristics for three types of annular gas seals operating in supercritical CO_2 turbomachinery. J Eng Gas Turbines Power 2021;143(10):101002.
[27] Yuan T, Li Z, Li J, Yuan Q. Design and analysis of cooling structure for dry gas seal chamber of supercritical carbon dioxide turbine shaft end. In: ASME turbo expo 2021: turbine technical conference and exposition. American Society of Mechanical Engineers; June .
[28] Wang W. Analysis of multi-axial creep–fatigue damage on an outer cylinder of a 1000 MW supercritical steam turbine. J Eng Gas Turbines Power 2014;136(11):112504.
[29] Xu X, Ma T, Li L, Zeng M, Chen Y, Huang Y, et al. Optimization of fin arrangement and channel configuration in an airfoil fin PCHE for supercritical CO_2 cycle. Appl Therm Eng 2014;70(1):867–75.
[30] Song J, Li X, Ren X, Gu C. Performance analysis and parametric optimization of supercritical carbon dioxide (S-CO_2) cycle with bottoming Organic Rankine Cycle (ORC). Energy 2018;143:406–16.
[31] Da LL, Manente G, Lazzaretto A. Predicting the optimum design of single stage axial expanders in ORC systems: is there a single efficiency map for different working fluids? Appl Energy 2016;167:44–58.
[32] Da LL, Manente G, Lazzaretto A. New efficiency charts for the optimum design of axial flow turbines for organic Rankine cycles. Energy 2014;77:447–59.
[33] Guo J, Li M, Xu J, Yan J, Ma T. Energy, exergy and economic (3E) evaluation and conceptual design of the 1000 MW coal-fired power plants integrated with S-CO_2 Brayton cycles. Energy Convers Manag 2020;211:112713.
[34] Wang Z, Zheng H, Xu J, Li M, Sun E, Guo Y, et al. The roadmap towards the efficiency limit for supercritical carbon dioxide coal fired power plant. Energy Convers Manag 2022;269:116166.
[35] Sun E, Xu J, Li M, Li H, Liu C, Xie J. Synergetics: the cooperative phenomenon in multi-compressions S-CO_2 power cycles. Energy Convers Manag X 2020;7:100042.
[36] Sun E, Xu J, Hu H, Li M, Miao Z, Yang Y, Liu J. Overlap energy utilization reaches maximum efficiency for S-CO_2 coal fired power plant: a new principle. Energy Convers Manag 2019;195:99–113.
[37] Li M, Wang G, Xu J, Ni J, Sun E. Life cycle assessment analysis and comparison of 1000 MW S-CO_2 coal fired power plant and 1000 MW USC water-steam coal-fired power plant. J Therm Sci 2020:1–22.
[38] Salah SI, Khader MA, White MT, Sayma AI. Mean-line design of a supercritical CO_2 micro axial turbine. Appl Sci 2020;10(15):5069.
[39] Lazzaretto A, Manente G. A new criterion to optimize ORC design performance using efficiency correlations for axial and radial turbines. Int J Therm 2014;17:173–81.
[40] Kacker SC, Okapuu U. A mean line prediction method for axial flow turbine efficiency. J Eng Power 1982;104:111–9.
[41] Marchionni M, Bianchi G, Tassou SA. Techno-economic assessment of Joule-Brayton cycle architectures for heat to power conversion from high-grade heat sources using CO_2 in the supercritical state. Energy 2018;148:1140–52.
[42] Deng Q, Jiang Y, Li J, Feng Z. Research on key technology of supercritical CO_2 power cycle experiment: power component. Therm Turb 2018;47(2):99–104 [in Chinese].
[43] Smith SF. A simple correlation of turbine efficiency. Aeronaut J 1965;69(655):467–70.
[44] Aungier RH. Turbine Aerodynamics: axial-flow and radial-inflow turbine design and analysis. New York (USA): ASME Press; 2005.
[45] Chu TL. Effects of mach number and flow incidence on aerodynamic losses of steam turbine blades. Doctoral dissertation. Faculty of the Virginia Polytechnic Institute and State University; 1997.
[46] Utamura M, Tamaura Y. A solar gas turbine cycle with super-critical carbon dioxide as a working fluid. In: ASME turbo expo 2006: turbine technical conference and exposition, Barcelona, Spain; 2006. p. 8–11. May.
[47] Macchi E, Perdichizzi A. Efficiency predictions for axial-flow turbines operating with nonconventional fluids. J Eng Power 1981;103:718–24.
[48] Dixon SL, Hall C. Fluid mechanics and thermodynamics of turbomachinery. Butterworth-Heinemann, Pergamon Press; 2013.
[49] Ainley DG, Mathieson GCR. A method of performance estimation for axial-flow turbines. In: British ARC, R&M 2974; 1951.
[50] Dunham J, Came PM. Improvements to the Ainley–Mathieson method of turbine performance prediction. J Eng Power 1970;92:252–6.
[51] Craig HRM, Cox HJA. Performance estimation of axial flow turbines. Proc Inst Mech Eng 1970;185(1):407–24.
[52] Balje OE, Binsley RL. Axial turbine performance evaluation. Part A—loss-geometry relationships. J Eng Power 1968:341–8.
[53] Shi D, Zhang L, Xie Y, Zhang D. Aerodynamic design and off-design performance analysis of a multi-stage S-CO_2 axial turbine based on solar power generation system. Appl Sci 2019;9(4):714.

[54] Dostal V. A supercritical carbon dioxide cycle for next generation nuclear reactors. Doctoral dissertation. Massachusetts Institute of Technology; 2004.
[55] Keep J, Jahn I. Numerical loss breakdown study for a small scale, low specific speed supercritical CO_2 radial inflow turbine. GPPS Montreal 2018;18:7–9.
[56] Hung TC, Shai TY, Wang SK. A review of organic Rankine cycles (ORCs) for the recovery of low-grade waste heat. Energy 1997;22(7):661–7.
[57] Fleming DD, Conboy TM, Pash JJ, Rochau GA, Fuller R, Holschuh TV, et al. In: Albuquerque NM, editor. Scaling considerations for a multi-megawatt class supercritical CO_2 brayton cycle and commercialization. November: Sandia National Laboratories; 2013.
[58] Sathish S, Kumar P, Namburi AN, Swami L, Fuetterer C, Gopi PC. Novel approaches for sCO_2 axial turbine design. In: ASME turbo expo 2019: turbine technical conference and exposition, Phoenix, Arizona, USA; June 17-21, 2019.